

UNIVERSIDAD TECNICA
FEDERICO SANTA MARIA

UNIVERSIDAD TÉCNICA FEDERICO SANTA MARÍA

UNDERGRADUATE THESIS

Electronic properties of graphene multilayers systems and behavior of localized states in twisted double ABC trilayer graphene.

Author:
Felipe Alejandro Pérez Riffo

Supervisor:
Dr. Eric Suárez Morell

A thesis submitted in fulfillment of the requirements
for the Bachelor in Physics
in the
Physics Department
Examination Committee:
Dr. Eric Suárez Morell
Dr. Francisco Peña
Dr. Juan Manuel Florez

February 14, 2024

"Life before death, strength before weakness, journey before destination."

Brandon Sanderson, *The Way of Kings*.

UNIVERSIDAD TÉCNICA FEDERICO SANTA MARÍA

Abstract

Physics Department

Bachelor in Physics

Electronic properties of graphene multilayers systems and behavior of localized states in twisted double ABC trilayer graphene.

by Felipe Alejandro Pérez Riffo

Interlayer rotation and stacking between the layers in two-dimensional atomic materials generates diverse properties and correlated phenomena. This work shows that by stacking two ABC trilayers with a rotation angle between them, transforms the system into a semiconductor with a gap about 30 meV. Flat bands persist even for large angles and the localization of electrons follows the same pattern as on trilayer ABC. A tight-binding model reveals the charge redistribution in the layers as a function of the angle. Below two degrees of rotation, the charge escapes from the rotated layers and AA zones and goes to the outer layers; this is a general trend for any trilayer ABA with one of the outer layers rotated. We explain this behavior with a simple toy model. Our findings shed light on some peculiarities of trilayer graphene and contribute to understanding correlated phenomena in graphene multilayers. This study advances knowledge on rotation, stacking, and electronic properties of two dimensional systems, paving the way for future applications.

Acknowledgements

I express my deepest gratitude to my family, whose unwavering support and encouragement have been my pillar throughout this academic journey. To my parents, siblings, and sister, your belief in me has been a constant source of inspiration. Their belief in me has been a driving force, and I am profoundly thankful for their constant presence.

Special appreciation goes to my guide professor, Dr. Eric Suarez, for his invaluable guidance, unwavering support, and trust in my abilities. From the outset, his insights and encouragement have played a pivotal role in shaping this research.

I extend heartfelt thanks to my friends and peers, both within and outside the university, for their camaraderie and understanding during challenging times. Their friendship has added immeasurable joy to my academic pursuits.

I am indebted to the dedicated educators who have imparted knowledge and wisdom, shaping my academic growth. Their passion for teaching and commitment to fostering learning have left an indelible mark.

A sincere acknowledgment is due to the members of the Grupo de Simulaciones, who graciously welcomed me into their community. Being part of this remarkable research group has been an enriching experience.

Lastly, I appreciate the collective efforts of all those who have played a role in my academic and personal development. Your contributions have been invaluable, and I am grateful for the collaborative spirit that has defined this journey.

Contents

Abstract ii

Acknowledgements iii

Contents iv

1 Introduction 1
- 1.1 General background: graphene isolation . . . 1
- 1.2 Evolution to graphene multilayers systems . . . 1
- 1.3 Outline . . . 2

2 Theoretical formalism 3
- 2.1 Carbon based structures . . . 3
- 2.2 Monolayer graphene . . . 4
  - 2.2.1 Tight-binding model . . . 5
- 2.3 Bilayer graphene . . . 6
  - 2.3.1 Tight-binding model . . . 7
- 2.4 Trilayer graphene . . . 8
  - 2.4.1 ABA and ABC stacking . . . 8
- 2.5 Twisted multilayers . . . 10
  - 2.5.1 Moiré superlattices . . . 11
  - 2.5.2 Unit cell . . . 11
  - 2.5.3 Tight-binding model . . . 14
  - 2.5.4 Band structure of twisted multilayers . . . 15
    - Twisted bilayer graphene . . . 15
    - Twisted double bilayer graphene . . . 16
- 2.6 Local density of states . . . 18
- 2.7 Electronic localization . . . 18
- 2.8 Structural lattice relaxation . . . 19
  - 2.8.1 LAMMPS molecular dynamics simulation . . . 19
- 2.9 Twisted double ABC trilayer graphene . . . 20

3 Results 22
- 3.1 ABC trilayer graphene . . . 22
- 3.2 Electronic properties of double twisted ABC trilayer . . . 23
  - 3.2.1 Band structure . . . 24
  - 3.2.2 Electronic localization for low angles . . . 26
    - Toy model . . . 29

4 Conclusion and outlook 30

A Monkhorst-Pack special points grid 31
- A.1 Crystal symmetry . . . 31

B Comparison of TB and DFT calculations **32**

Bibliography **33**

To my family...

Chapter 1

Introduction

1.1 General background: graphene isolation

Since the experimental isolation of graphene by mechanical exfoliation in 2004 by Novoselov et al. [1], the field of materials science has experienced exceptional progress. Andre Geim and Konstantin Novoselov won the 2010 Nobel Prize in Physics for their groundbreaking work on graphene. To date, new techniques for the synthesis of graphene monolayers have been developed, such as mechanical exfoliation, thermal decomposition of SiC, chemical vapor deposition, molecular beam deposition, and unzipping carbon nanotubes [2]. In the period 2005-2010 alone, more than 5000 articles were published on the electronic properties of graphene [3], evidencing the rapid interest of the scientific community in understanding the characteristics of this new material. The fast uptake of interest in graphene is due primarily to a number of exceptional properties that it has been found to possess. These properties range from the observation of the integer quantum hall effect [4], excellent conducting properties, to the fact that the charge carriers in the monolayer are massless chiral quasiparticles with a linear dispersion, as described by a Dirac-like effective Hamiltonian.

1.2 Evolution to graphene multilayers systems

This initial phase of research laid the groundwork for the exploration of more complex systems. Interest naturally expanded to graphene bilayers, where two monolayers are stacked. This study provided insight into how interlayer interactions affect electronic properties. Such interactions cause the charge carriers in the bilayer at low energies to behave as massive chiral quasiparticles, with parabolic dispersion. Eventually the study was extended to multilayer systems, with a range of possibilities of stacking each monolayer one on top of the other and with this, the appearance of superconducting and correlation phenomena in various systems, which will be discussed in the next chapter.

In addition to the study of multilayers, the study of a new branch called *twistronics* arises, in which in addition to the stacking of the layers, a rotation between them is introduced, and with this new properties of interest appear that the monolayers separately or the multilayers without rotation do not possess, expanding the range of possibilities of study in the physics of two-dimensional materials.

The introduction of rotation in layered structures introduces a remarkable degree of tunability in electronic, optical, and even mechanical properties. By altering the angle of rotation, researchers gain unprecedented control over the interlayer coupling, leading to the emergence of moiré patterns and flat electronic bands. The

interplay between stacking order and rotation angle becomes a pivotal factor, opening up an expansive landscape for the exploration of correlated electron phenomena and the manipulation of material properties.

Notably, the *twistronics* framework has demonstrated its potential in generating unconventional superconductivity, Mott insulating states, and other intriguing phases, providing a rich playground for researchers to delve into emergent quantum behaviors. This dynamic interplay between rotation and stacking has propelled *twistronics* into the forefront of materials science, offering a promising avenue for tailoring the properties of two-dimensional materials with unprecedented precision. The ensuing chapters will delve deeper into the outcomes of this exciting exploration, shedding light on the intricate interplay between rotation, stacking, and the resulting electronic properties.

1.3 Outline

This thesis are organized as follows: Chapter 2 starts with a general review of the mathematical formalism of systems based on graphene monolayers, starting from the study of a single monolayer, to the study of rotated multilayer systems, reviewing the tight-binding models used and the band structures obtained from this model for the different systems that serve as a basis for the main objective of this work. Then in Chapter 3 the main results of this thesis are presented, and specifically the electronic and transport properties of a twisted double ABC trilayer graphene, together with the subsequent analysis of its band structure and charge distribution. Finally in Chapter 4 the conclusions drawn from the results are discussed, offering insights into the implications of these findings and outlining potential avenues for future research in this field.

Chapter 2

Theoretical formalism

This chapter delves into the theoretical foundations essential for understanding the electronic intricacies of graphene multilayers and their twisted counterparts. We commence this exploration with an overview of carbon-based structures, from monolayer graphene to intricate twisted multilayers. The section unfolds with a focus on tight-binding models, providing a fundamental framework for comprehending the electronic behavior at various structural levels.

The subsequent discussions encompass bilayer and trilayer graphene, detailing stacking arrangements like ABA and ABC. As we navigate through the theoretical landscape, the emergence of twisted multilayers introduces moiré superlattices and a nuanced examination of the band structure. This comprehensive journey culminates in an exploration of electronic localization, local density of states, and structural lattice relaxation. The chapter concludes with an introduction to the specific system under scrutiny – twisted double ABC trilayer graphene. Through this theoretical lens, we lay the groundwork for unraveling the intriguing electronic phenomena presented in subsequent chapters.

2.1 Carbon based structures

Systems made of carbon atoms are of particular interest for the study of a large variety of physical properties, due the flexibility of its bonding. These physical properties emerges, in gran part, because of the dimensionality of these structures. Among these systems, the monolayer graphene, a 2D allotrope of carbon, play an important role, since it can be viewed as the basis for all the others systems based on carbon atoms; such as fullerenes, nanotubes and multilayers graphene structures [5, 6].

In addition to their fundamental importance, carbon systems exhibit exceptional mechanical properties, strength and fascinating electronic and optical properties. Research in this area has experienced a significant increase in interest, highlighting recent discoveries that have broadened our understanding of these materials. In a broader context, carbon-based structures have potential applications in technological fields such as nanotechnology, advanced electronics and the exploration of new energy sources.

To better understand these properties, it is essential to have insight into the underlying atomic structure. In the case of graphene, its unique hexagonal arrangement of carbon atoms contributes fundamentally to its exceptional properties. In this chapter, we will explore in detail various carbon structures, from graphene to multilayer graphene structures, and discuss their physical, electronic, and structural properties.

2.2 Monolayer graphene

Graphene is a two-dimensional lattice with carbon atoms arranged in a hexagonal honeycomb lattice. This structure can be seed as a triangular Bravais lattice with a basis of two inequivalents atoms in the unit cell, denoted by A and B, as are shown in Figure 2.1. This inequivalence can be see considering their nearest neighbour vectors, wich require a parity flip (i.e, the position vector transforms from $\mathbf{r} \to -\mathbf{r}$) between A and B sites. The primitive lattice vectors are

$$\mathbf{a}_1 = \frac{a}{2}\left(3, \sqrt{3}\right), \quad \mathbf{a}_2 = \frac{a}{2}\left(3, -\sqrt{3}\right), \tag{2.1}$$

where $a = 1.42$ Å is the distance between carbon atoms. The reciprocal lattice vectors are therefore

$$\mathbf{b}_1 = \frac{2\pi}{3a}\left(1, \sqrt{3}\right), \quad \mathbf{b}_2 = \frac{2\pi}{3a}\left(1, -\sqrt{3}\right). \tag{2.2}$$

Each lattice site has three nearest neighbors, separated by

$$\delta_1 = \frac{a}{2}\left(1, \sqrt{3}\right), \quad \delta_2 = \frac{a}{2}\left(1, -\sqrt{3}\right), \quad \delta_3 = -a(1, 0), \tag{2.3}$$

while the six second-nearest neighbors are located at $\delta_1' = \pm\mathbf{a}_1$, $\delta_2' = \pm\mathbf{a}_2$ and $\delta_3' = \pm(\mathbf{a}_2 - \mathbf{a}_1)$.

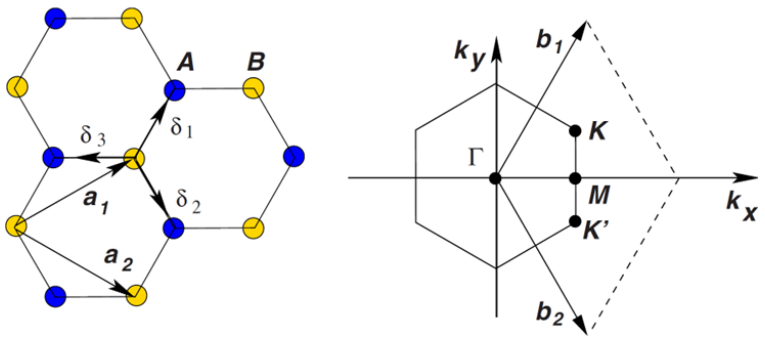


FIGURE 2.1: Hexagonal lattice of graphene and its Brillouin zone. Left: lattice structure of graphene, made out of two interpenetrating triangular lattices, with $\mathbf{a}_{1,2}$ are the lattice vectors; and $\delta_{1,2,3}$ are the nearest-neighbor vectors of the atoms in the unit cell. Right: corresponding Brillouin zone with reciprocal lattice vectors $\mathbf{b}_{1,2}$ and the high simmetry points [5].

The high symmetry points M, K and K' are located at the corners of the graphene Brillouin zone (BZ). The points K and K' are referred to as the Dirac points or "valleys" due to the dispersion relations of graphene around these points, which we shall see later. Their positions in momentum space are given by

$$\mathbf{M} = \frac{2\pi}{\sqrt{3}a}(1, 0), \quad \mathbf{K} = \frac{2\pi}{3a}\left(1, \frac{1}{\sqrt{3}}\right), \quad \mathbf{K}' = \frac{2\pi}{3a}\left(1, -\frac{1}{\sqrt{3}}\right). \tag{2.4}$$

In the BZ exists three equivalents K points and three equivalent points K'; the inequivalent between the K and K' points is associated to two inequivalent lattice sites in the unit cell.

Each carbon atom have six electrons, two of which are in the core 1s orbital and can be disregarded as they do not contribute to bonding or transport. The remaining

four are in the outer 2*s*-2*p* orbital shells, and the fundamental key to the structural and electronic properties of graphene and other structures lies on the sp^2 hybridisation between the *s* and *p* orbital electrons [2, 5, 7]. The *s*, p_x and p_y orbitals hybridise, and this combination forms the σ-bond between atoms. These σ-bonds between carbon atoms are separated by 1.42 Å, and oriented with mutual angles of 120° in the *xy*-plane, producing a trigonal planar structure. The remaining unhybridised p_z electron orbital, which is oriented in the *z*-direction (out of the plane) forms covalent bonds with neighbouring atoms, constituting the π-bond. Each atom has one of these π-bonds, which are then hybridized together to form what are known as the π-band and π^*-bands [2], which plays a fundamental role in the most of the electronic properties of graphene.

2.2.1 Tight-binding model

In tight-binding (TB) approximation, the electronic spectrum of graphene can be derived by considering the π orbitals and charge carriers hopping from lattice sites to their nearest and next-nearest neighbouring atoms [5]. Therefore, the appropiate tight-binding Hamiltonian is

$$\mathcal{H} = -\gamma_0 \sum_{\langle i,j \rangle} \left(a^\dagger_{\sigma,i} b_{\sigma,j} + H.c. \right) - t' \sum_{\langle\langle i,j \rangle\rangle,\sigma} \left(a^\dagger_{\sigma,i} a_{\sigma,j} + b^\dagger_{\sigma,i} b_{\sigma,j} + H.c. \right), \tag{2.5}$$

where $a^\dagger_{\sigma,i}(a_{\sigma,i})$ create (annihilates) an electron with spin $\sigma(\sigma = \uparrow, \downarrow)$ on site $\mathbf{R}_i$ on sublattice A (an equivalent definition for the sublattice B), γ_0 is the nearest-neighbor hopping energy between different sublattices and t' is the next-nearest neighbor hopping energy in the same sub-lattice. The value of γ_0 used in the literature is $\gamma_0 \approx 2.7$ eV, and the value for t' can be derived by *ab initio* calculations, from which it has been found that $0.02\gamma_0 \leq t' \leq 0.2\gamma_0$ [5].

The solution of this Hamiltonian give us the dispersion relation for the energy, given by

$$E_\pm(\mathbf{k}) = \pm\gamma_0 \sqrt{3 + f(\mathbf{k})} - t' f(\mathbf{k}), \tag{2.6}$$

where $f(\mathbf{k})$ is

$$f(\mathbf{k}) = 2\cos\left(\sqrt{3}k_y a\right) + 4\cos\left(\frac{\sqrt{3}}{2}k_y a\right)\cos\left(\frac{3}{2}k_x a\right), \tag{2.7}$$

and *a* is the lattice constant. This dispersion relation is shown in Figure 2.2. Positive energy states correspond to the π^* band an negative states to the π band. A zoom-in on the *K* point reveal a band touching with a lineal dispersion. Thus, graphene monolayer is a gap-less semiconductor, with a linear, rather than quadratic, long wavelength energy dispersion.

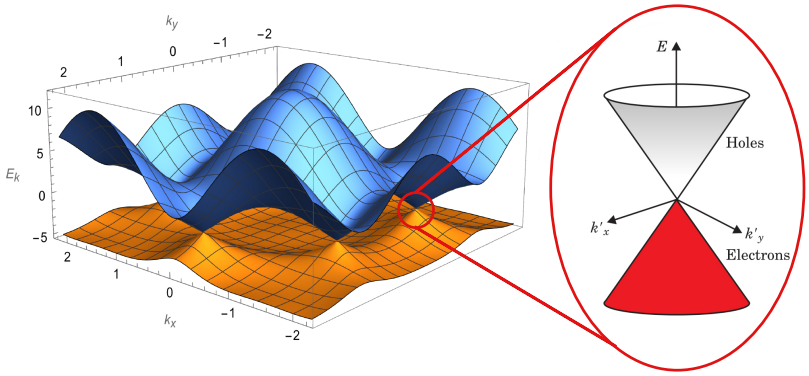


FIGURE 2.2: Band structure of graphene monolayer. Left: Dispersion relation for graphene monolayer. Right: Zoom-in on the Dirac point K, representing the Dirac cone and the linear dispersion near this point. Adapted from [3].

Expanding the Hamiltonian (2.5) near the $K(K')$ point and neglecting t' gives the following effective Hamiltonian

$$H = \hbar v_F \begin{pmatrix} 0 & k_x - ik_y \\ k_x + ik_y & 0 \end{pmatrix} = \hbar v_F \boldsymbol{\sigma} \cdot \mathbf{k}, \tag{2.8}$$

where k is the momentum of the quasi-particle measured respect the Dirac points, $\boldsymbol{\sigma}$ are the Pauli matrices and v_F is the graphene charge carriers velocity, which has a value of $v_F \approx c/300$, with c the light velocity. This Hamiltonian is called Dirac-like, because the similarity with the description of electron in high-energy physics. Therefore, equation (2.8) is the equation for mass less chiral Dirac fermions in 2D where the speed of light has been replaced by v_F. Many of the interesting properties of graphene can be mapped back to this unique dispersion.

2.3 Bilayer graphene

Bilayer graphene (BG) consist in a two monolayers placed one on top of the other. The unit cell of the bilayer contains four atoms, labelled $A1, B1$ on the lower layer and $A2, B2$ on the upper layer. The stacking of the layers are called Bernal or "AB", and is such that one of the atoms A_i from the upper(lower) layer, has directly an atom below(above) it from the other layer, as is shown in Figure 2.3. In contrast, type B_i atoms have neither upper nor lower neighbors. In general, three atoms of the hexagon are of type A and three are of type B. The lattice vectors of this structure are the same of the monolayer: $\mathbf{a}_1 = \frac{a_0}{2}\left(-1, \sqrt{3}\right)$, $\mathbf{a}_2 = \frac{a_0}{2}\left(1, \sqrt{3}\right)$, where $a_0 = 2.42$ Å. In addition, the bilayer is symmetric with respect to spatial inversion symmetry $(x, y, z) \to (-x, -y, -z)$ [8–10]. The distance between layers is $c \approx 3.35$ Å.

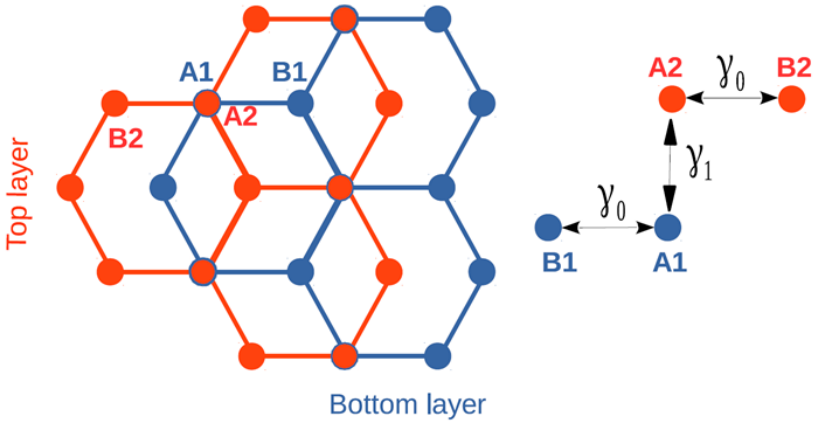


FIGURE 2.3: Left: Top view of the BG. Right: Side view of the unit cell of BG.[11]

2.3.1 Tight-binding model

The tight-binding model for bilayer graphene can be constructed considering $2p_z$ orbitals on the four atomic sites of the unit cell, labelled as $j = A1, B1, A2, B2$ [8]. Then, the matrix of the tight-binding Hamiltonian is given by

$$H = \begin{pmatrix} V & -\gamma_0 f(\mathbf{k}) & \gamma_1 & -\gamma_3 f(\mathbf{k}) \\ -\gamma_0 f^*(\mathbf{k}) & V & -\gamma_3 f^*(\mathbf{k}) & 0 \\ \gamma_1 & -\gamma_3 f^*(\mathbf{k}) & -V & -\gamma_0 f(\mathbf{k}) \\ -\gamma_3 f(\mathbf{k}) & 0 & -\gamma_0 f^*(\mathbf{k}) & -V \end{pmatrix}, \tag{2.9}$$

where V is the potential in both layers, and the hoppings terms (see Figure 2.3(b)) are defined as:

$$\gamma_0 = \langle \phi_{A1} | \mathcal{H} | \phi_{B1} \rangle = \langle \phi_{A2} | \mathcal{H} | \phi_{B2} \rangle , \tag{2.10}$$
$$\gamma_1 = \langle \phi_{A1} | \mathcal{H} | \phi_{A2} \rangle , \tag{2.11}$$
$$\gamma_3 = \langle \phi_{A1} | \mathcal{H} | \phi_{B2} \rangle = \langle \phi_{B1} | \mathcal{H} | \phi_{A2} \rangle , \tag{2.12}$$

where ϕ_j are the orbital on the different lattice sites and $\mathcal{H}$ is the Hamiltonian. In other words, the hopping γ_0 represent the interaction between the atoms on the same layer, γ_1 the overlap to nearest-neighbors between different layers and γ_3 the next-nearest neighbors hopping.

The band structure of the bilayer graphene obtained from equation (2.9) is shown in the left side of Figure 2.4. Plots were made using the following tight-binding parameters: $\gamma_0 = -2.65$ eV, $\gamma_1 = 0.48$ eV, $\gamma_3 = 0$ eV, $V = 0$ eV. Is clear the parabolic dispersion near the $K(K')$ points, unlike de lineal dispersion seen in the monolayer (see Figure 2.1). Thus, the bilayer graphene is a gapless semiconductor, and, moreover, this gap can be tunable with an external potencial perpendicular to the layers, as is shown in the right side of the Figure 2.4). This tunability in the gap has been experimentally proven by several groups, both from an applied external field [12–14] as well as from a molecular doping of the layers [15, 16]. This ability to open a gap makes bilayer graphene interesting for technological applications. Moreover, in Bernal bilayer graphene has been found experimental evidence of isospin magnetism and spin-polarized superconductivity [17], and a enhanced of superconductivity by placing tungsten diselenide (WSe_2) on top of the bilayer [18]; the interplay

with WSe_2 leads to a significant, global enhancement of superconductivity: it appears even in the absence of a magnetic field.

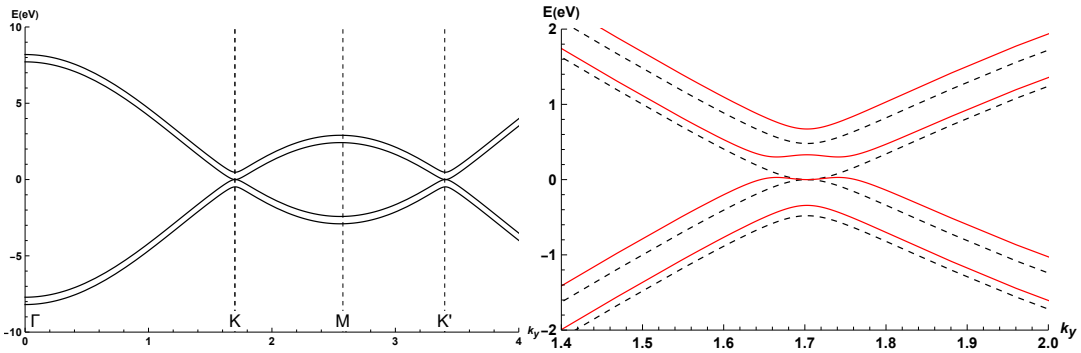


FIGURE 2.4: Left: Band structure of bilayer graphene (eq.(2.9)). Right: Zoom in to the Dirac point and comparison of the bands for an applied external potencial.

2.4 Trilayer graphene

Trilayer graphene consists of three monolayers stacked one of top of each other. The basis stacking of the two lowers layers is AB or Bernal, so that we find two possible configurations for the trilayer emerge depending on how the upper layer is arranged. Each one of them has a completely different electronic properties. In the following sections we detail their structure and the corresponding dispersion relation obtained from the tight-bindig model.

2.4.1 ABA and ABC stacking

Starting with a Bernal stacking, its possible to construct two types of trilayer: ABA or Bernal, and ABC or rhombohedral. The ABA stacking of the layers, shown in Figure 2.5(a), is such that the atoms of the topmost layer lies exactly on top of those of the bottom layer, and have mirror reflection symmetry about the center layer along the z-direction. In the ABC stacking, one sublattice of the top layer lies above the centre of the hexagons in the bottom layer, as is shown in Figure 2.5(b). In addition, ABC trilayer posseses inversion symmetry, but lacks mirror symmetry.

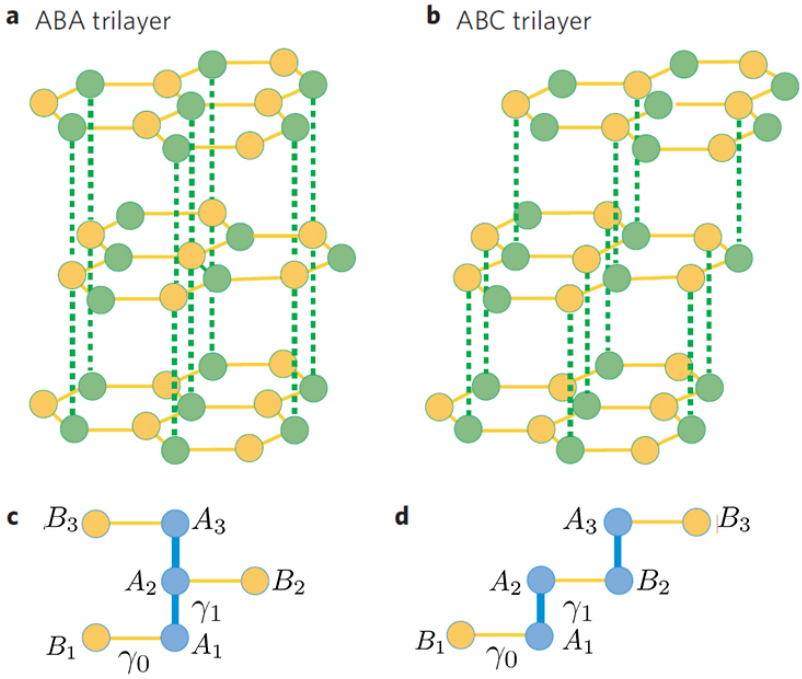


FIGURE 2.5: (**a**) Structure of ABA trilayer graphene. **(b)** Structure of ABC trilayer graphene. **(c)** Tight-binding diagram for ABA trilayer. **(d)** Tight-binding diagram for ABC trilayer. [19].

To obtain the band structure of the trilayers, a tigth-binding Hamiltonian can be constructed in a similar way to the bilayer. Basically consist in constructing the following matrix Hamiltonian

$$H = \begin{pmatrix} H_1 & T & T' \\ T^* & H_2 & T \\ (T')^* & T^* & H_3 \end{pmatrix}, \tag{2.13}$$

where $H_i, i = 1, 2, 3$ are the monolayer tight-binding Hamiltonians, and T, T' are the interacting matrix between the layers. As in shown in Figures 2.5(c) and 2.5(d), only the parameter γ_0 between the same layer and γ_1 between direct neighbors between layers are considered.

The band structure of the trilayers near the K point are shown in Figure 2.6. On one hand, the energy dispersion of ABA trilayer consists of both monolayer-like and bilayer-like subbbands, and an application of an external potential does not open a gap, and moreover, increase the overlapping between the bands. On the other hand, the ABC stacking present a zero gap band structure without a external field, but the presence of a potential perpendicular to the layers can possibly open and control the gap. These effects have been studied both theoretically [20–22] and experimentally [19, 23–28], confirming the controllability of the gap in the ABC trilayer, as well as the no gap-opening for the ABA trilayer.

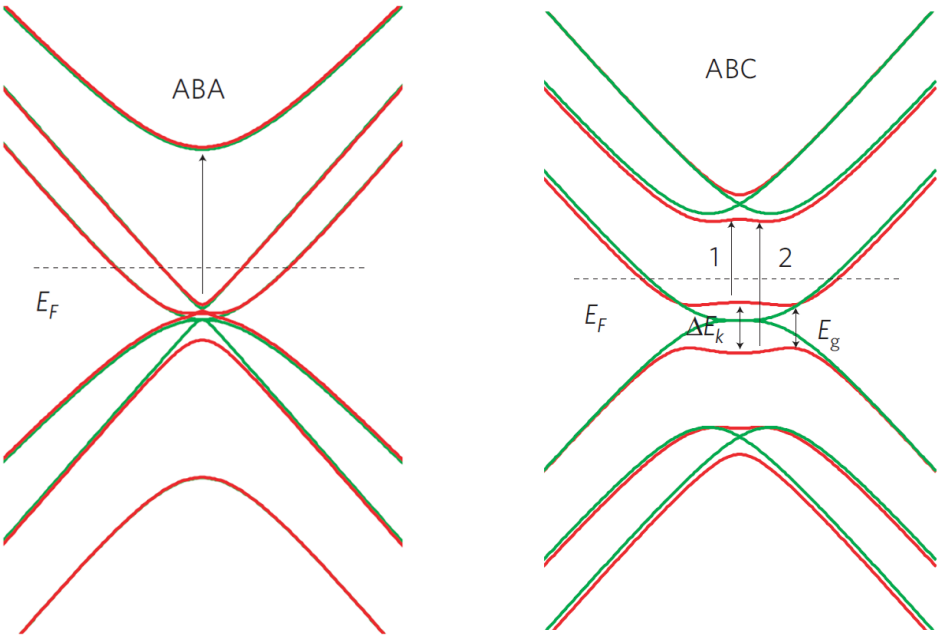


FIGURE 2.6: Left: Band structure of ABA trilayer graphene. Right: Band structure of ABA trilayer graphene with optical transitions. In green are shown the dispersion relation without a external potential, and in red the dispersion with an external field perpendicular to the layers. [19].

In addition to the properties explained above, recently, has been found superconductivity in the ABC trilayer graphene [29]. This group found experimental evidence of two superconductivity regions, called SC1 and SC2, and arise near a phase transition break in the system. This superconductivity emerges at temperatures below Kelvin, where it reaches values between 90-150 mK for SC1 and up to 20 mK for SC2. A dependence of this superconductivity on the applied external magnetic field, both perpendicular and parallel to the layers, is also observed. Several theories have been proposed to account the effective interaction between electron in this superconducting state: electron-phonon coupling [30], spin fluctuations near an antiferromagnetic phase [31, 32], direct coupling by the screened Couloumb interaction [33], pairing mediated by the proximity to a correlated insulator [34], or repulsive interactions due to the long-range Coulomb repulsion [35].

2.5 Twisted multilayers

In the preceding sections, we delved into the theoretical formalism of monolayer and multilayer graphene without introducing relative rotation between the layers. However, when these layers are stacked with a certain rotation angle between them, an intriguing set of electronic properties emerges, giving rise to a novel network known as moiré superlattices. This phenomenon has become a focal point of investigation due to the unique electronic structures it engenders.

The introduction of a relative rotation angle between layers introduces a new dimension to the electronic properties of these systems, presenting an exciting avenue for exploration. This section aims to develop the theoretical framework for understanding these rotated multilayer systems. We will explore the construction of new unitary supercells to accommodate the rotation and elaborate on the tight-binding

model to be employed. Furthermore, we will delve into the detailed electronic properties of various rotated multilayer systems.

The study of twisted multilayers is not only an extension of our previous work on non-rotated structures but also a crucial exploration into a realm where new phenomena and behaviors manifest. Researchers are drawn to these systems for their potential applications in diverse fields, ranging from electronics to materials science. Recent advances in this area have unveiled exciting possibilities, and as we delve into this section, we will also touch upon current challenges and open questions that drive the ongoing exploration of these fascinating structures.

2.5.1 Moiré superlattices

Moiré superlattices arise from the intricate interplay of two-dimensional materials, such as graphene, when stacked with a specific angle of rotation between them. This unique configuration gives rise to Moiré patterns, characterized by a much higher periodicity than that observed in the parent graphite structure. The formation of Moiré patterns is a visually striking manifestation of the quantum mechanical interference between the layers, leading to a modulation in the local electronic density and potential landscape.

These Moiré superlattices are not merely aesthetic; rather, they bring forth a plethora of fascinating electronic properties that are absent in the individual layers themselves. The rotational alignment introduces a new level of complexity, resulting in phenomena such as superconductivity, magnetism, topological edge states, and correlated insulator phases [36–38]. Understanding and manipulating these emergent properties has become a key focus of research, driven by the potential applications in various technological domains.

To delve deeper into the intricacies of Moiré superlattices, it is crucial to explore specific examples of these emergent properties. For instance, recent studies have unveiled the coexistence of superconductivity and correlated insulator phases in certain twisted bilayer graphene configurations, providing valuable insights into the rich tapestry of phenomena that can be engineered through precise control of stacking and rotation angles [39, 40].

As we embark on the exploration of graphene multilayer systems with different stacking arrangements and interlayer rotations in the subsequent sections, our aim is to unravel the electronic nature of these materials and contribute to the expanding knowledge base of these unique and promising structures.

2.5.2 Unit cell

To build the new unitary supercell, one can start from the simplest system in this case: the Twisted Bilayer Graphene (TBG). Then, the procedure for the TBG can be generalized to more layers in a simple way.

We initially start with two graphene layers in a Bernal or AB stacking, and a site B is selected as the axis of rotation. This rotation is made in a commensurable way. First, an atom is taken, from the layer to be rotated, which is in the position $\mathbf{r} = m\mathbf{a}_1 + n\mathbf{a}_2$ with respect to the rotation axis, and we take it to position $\mathbf{t}_1 = n\mathbf{a}_1 + m\mathbf{a}_2$, also site of the initial lattice; where m and n are two integers. It directly follows that the vectors $\mathbf{r}$ and $\mathbf{t}_1$ have the same modulo. This procedure is schematized in Figure 2.7(a).

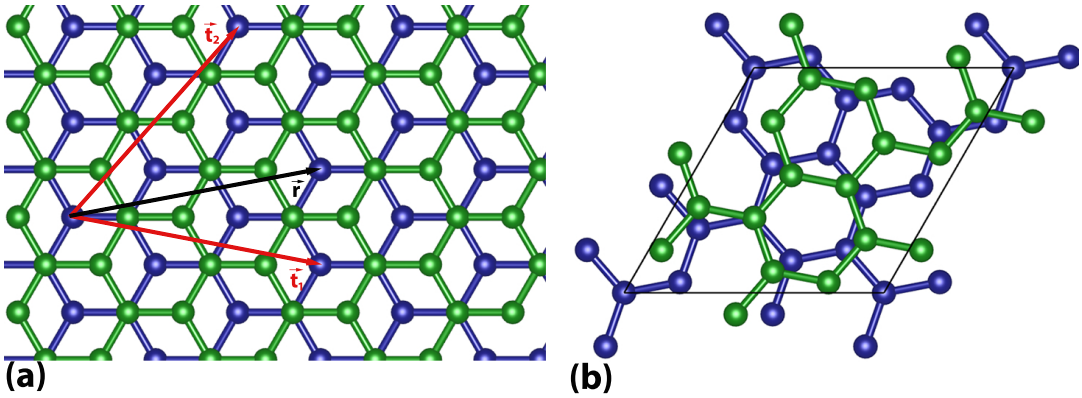


FIGURE 2.7: (**a**) Unit cell construction from an AB stacking. **(b)** Unit cell of TBG with 28 atoms and a rotation angle of 21.8°.

If m and n are taken so that they are not divisible by each other we can choose the vector $\mathbf{t}_1$ as one of the unit vectors of the supercell. This vector joint two equivalents points in the new supercell, there not existing any other point of the previous lattice in the same direction according to the choice of m and n, and a new equivalent point in that direction will necessarily be an integer multiply of $\mathbf{t}_1$. This will allow, as will be shown below, to obtain as a function of the lattice vectors of graphene and of m and n the important quantities that characterize the unit cell as well as its Brillouin zone.

Graphite has C_6 rotational symmetry with respect to an axis perpendicular to it, which means that a rotation of 60° of one of the layers recovers the initial state. Furthermore, it can be shown that symmetric configurations around 30° are obtained, so that only angles between 0 and 30° will be of interest for the calculation of the electronic properties. The new supercell obtained after the rotation have the same symmetry C_6, so the second unit vector will be the one obtained by rotating $\mathbf{t}_1$ in 60°. Thus, the two unit vectors of the new unit supercell will be given by

$$\mathbf{t}_1 = n\mathbf{a}_1 + m\mathbf{a}_2, \quad \mathbf{t}_2 = -m\mathbf{a}_1 + (n+m)\mathbf{a}_2, . \tag{2.14}$$

with the same magnitud and equal to

$$|\mathbf{t}_i| = \sqrt{n^2 + mn + m^2}a_0, \quad i = 1, 2. \tag{2.15}$$

The rotation angle θ between the layers can be obtained by the angle between the vectors $\mathbf{r}$ and $\mathbf{t}_1$, and can be calculated from:

$$\cos(\theta) = \frac{n^2 + 4mn + m^2}{2(n^2 + mn + m^2)}. \tag{2.16}$$

To calculate the number of atoms inside the unit supercell from the unit vectors $\mathbf{t}_1$ and $\mathbf{t}_2$, first calculate the area expanded by these vectors, and then divide it by the area of the unit cell of the bilayer graphene, and finally multiply it by the number of atoms in the unit cell of the bilayer graphene, which is 4, obtaining finally

$$N = 4(n^2 + mn + m^2). \tag{2.17}$$

For more layers, it should be multiply by the number of atoms in the unit cell of that configuration without rotating, for example for the trilayer multiply by 6, for four layers multiply by 8 and so on.

The reciprocal lattice vectors are then given by

$$\mathbf{G}_1 = \frac{2\pi}{\sqrt{3}a_0(n^2+mn+m^2)}(n+2m, -n\sqrt{3}), \tag{2.18}$$

$$\mathbf{G}_2 = \frac{2\pi}{\sqrt{3}a_0(n^2+mn+m^2)}(n-m, (n+m)\sqrt{3}). \tag{2.19}$$

It directly follows the position of the high symmetry points K and M in the first Brillouin zone, given respectively by

$$K = \frac{2\pi}{\sqrt{3}a_0(n^2+mn+m^2)}((n+m)\sqrt{3}, m-n), \tag{2.20}$$

$$M = \frac{\pi}{\sqrt{3}a_0(n^2+mn+m^2)}(n+2m, -n\sqrt{3}). \tag{2.21}$$

The supercell for a rotation of 21.8°, with $n = 2$ and $m = 1$ is composed of 28 atoms, as is shown in Figure 2.7(b). Neverthless, the supercell for a smaller angle of 2.45° have 2188 atoms, this makes it difficult to calculate the electronic properties of these supercells by first-principles methods.

The choose for n and m is in principle arbitrary, only with the condition that are indivisible by each other; but in this work we choose $m = n - 1$. In Figure 2.8 is shown the unit cell of TBG for $n = 4$ and $m = 3$.

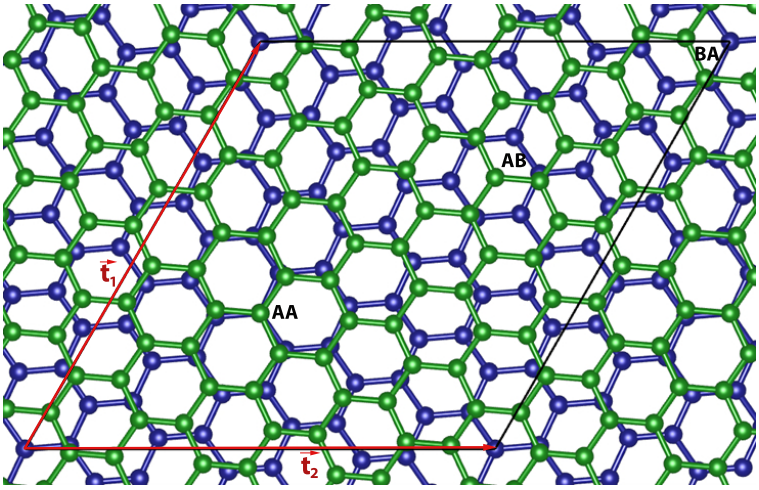


FIGURE 2.8: Unit supercell for TBG with a rotation angle $\theta = 9.43°$ and $N = 148$ atoms. AA, AB and BA sites are highlighted.

With this election of n and m, it is clear to note that at one third of the diagonal of the unit cell there is an AA site, at two thirds of the diagonal an AB site, and at the ends of the cell there are BA sites. The difference between an AB site and a BA site is that at the AB, an atom A is in the upper layer and in the BA the atom A in in the lower layer. it can be shown that this is true for any n and m. There are other sites of interest in the unit cell, which are intermediate between an AA site and an AB or BA site. This sites are called SL (slip). It is possible to classify a site like AA if the horizontal difference between the two atoms is less than δ, and the same for a AB (BA) site, in that case when the atom in the upper (lower) layer is at distance less than δ to te center of the hexagon of the bottom layer, where δ is a small parameter; sites that do not comply with these two conditions will be classified as SL.

Evidently, the numbers of types in the unit cell will vary according to the angle of rotation chosen. In Figure 2.9 is shown the relative abundance of AA, BA and SL sites in the unit cell in depende of the relative rotation angle (RRA). It is clear that for angles near to 30° the sites in de unit cell then most of the sites are SL. However, for small angles the number of SL sites decreases markedly, while BA and AA sites grow, and most of them are BA sites.

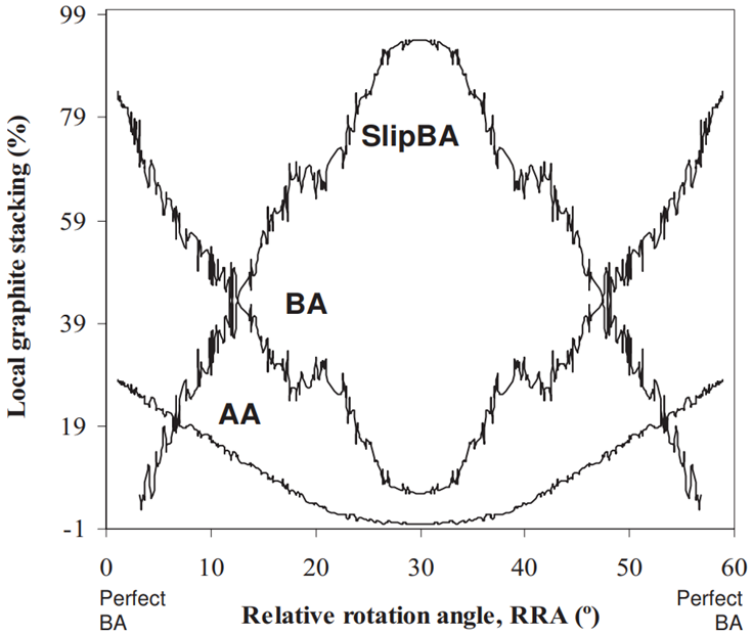


FIGURE 2.9: Percentage of abundance of AA, AB and SL type sites in the rotated unit cell as a function of angle [41].

2.5.3 Tight-binding model

The tight-binding model for twisted multilayers at low angles of rotation is obtained using the model of Nam and Koshino [42]. The Hamiltonian is written as

$$\mathcal{H} = \sum_i \Delta_i \left|\mathbf{R}_i\right\rangle\!\left\langle\mathbf{R}_j\right| - \sum_{i,j} t(\mathbf{R}_i - \mathbf{R}_j) \left|\mathbf{R}_i\right\rangle\!\left\langle\mathbf{R}_j\right| + H.c., \tag{2.22}$$

where $\mathbf{R}_i$ is the atomic coordinate, $|\mathbf{R}_i\rangle$ is the wave function at site i, $\Delta_i = \pm 20$ meV is the on-site term that takes a positive or negative value, depending on the layer; this term is added to the model to address the crystal field related to a charge transfer between layers; and $t(\mathbf{R}_i - \mathbf{R}_j)$ is the transfer integral between atoms i and j, given by

$$-t(\mathbf{d}) = V_{pp\pi}(d)\left[1 - \left(\frac{\mathbf{d}\cdot\mathbf{e}_z}{d}\right)^2\right] + V_{pp\sigma}(d)\left(\frac{\mathbf{d}\cdot\mathbf{e}_z}{d}\right)^2, \tag{2.23}$$

and the explicit expression for the hopping parameters are

$$V_{pp\pi}(d) = V^0_{pp\pi}\exp\left(-\frac{d-a_0}{r_0}\right), \tag{2.24}$$

$$V_{pp\sigma}(d) = V^0_{pp\sigma}\exp\left(-\frac{d-d_0}{r_0}\right), \tag{2.25}$$

where $\mathbf{d} = \mathbf{R}_i - \mathbf{R}_j$ is the distance between two atoms, and $\mathbf{e}_z$ is the unit vector on the z axis, $V^0_{pp\pi} \approx -2.65$ eV is the transfer integral between nearest-neighbor atoms of monolayer graphene which are located at distance $a_0 = a/\sqrt{3} \approx 1.42$ Å, $V_{pp\sigma} \approx 0.48$ eV is the transfer integral between two nearest vertically aligned atoms, $d_0 \approx 3.34$ Å is the interlayer spacing and $r_0 = 0.184a$ is the decay length of the interaction, with a being the interatomic distance.

2.5.4 Band structure of twisted multilayers

This section will describe the band structure of two rotated multilayer systems, which serve as the basis for the main system of this thesis.

Twisted bilayer graphene

The construction of the TBG is was shown in the section 2.5.2. It is logical to ask how the electronic properties of this rotated system change in comparison with the monolayer and the Bernal bilayer stacking.

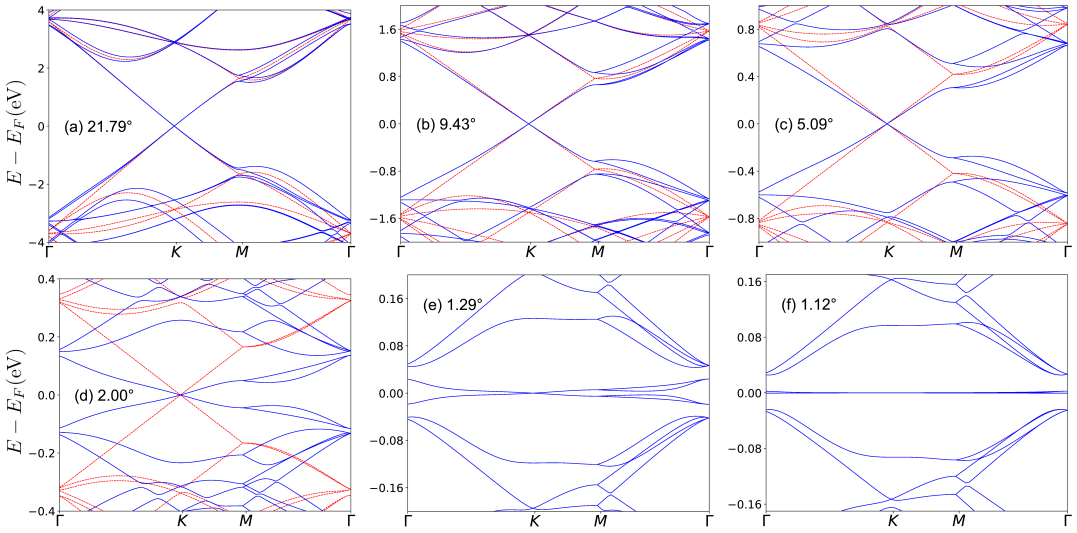


FIGURE 2.10: Band structure of TBG (blue solid line) for six different rotation angles: (a) 21,79°, (b) 9.43°, (c) 5.09°, (d) 2.00°, (e) 1.29° and (f) 1.12°. In red dashed line is shown the band structure of graphene monolayer for comparision.

In Figure 2.10 is shown the band structure obtained from the TB model through the points $\Gamma - K - M - \Gamma$ in the Brillouin Zone for six different rotation angles between the layers. For large angles, like in Fig. 2.10(a), (b) and (c), the the dispersion is lineal near the K point, similar to what is observed in the graphene monolayer, as is shown in red dashed lines. Moreover, the slope of the dispersion for the TBG is always smaller than the monolayer, and as we will see below, this is related to the velocity of the charge carriers in the twisted bilayer. For small angles close to 1°, a rapid flattening of the bands is observed, where the slope of the linear dispersion for the TBG approaches zero. For a rotation angle of 1.12°, the bands near the Fermi level are completely flat.

This flat bands for low angles are related with a decrease in the Fermi velocity of the charge carriers. They are of great importance in the study of two-dimensional

materials, since they are related to superconductivity, phase transitions and correlation phenomena between electrons belonging to these bands [43, 44].

A renormalization of the Fermi velocity can be obtained from the quotient between the Fermi velocity in TBG and the corresponding Fermi velocity in monolayer graphene, $v_F^{(TBG)}/v_F^{(G)}$, as a function of the twisting angle. This relation is plotted in Figure 2.11.

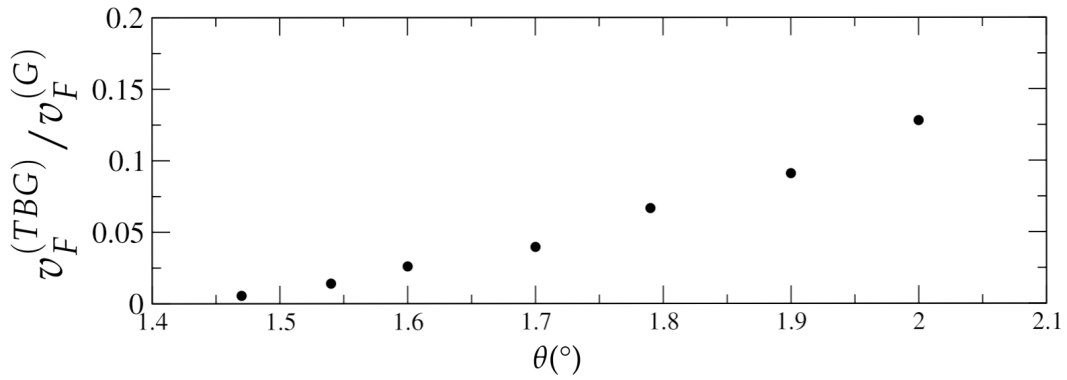


FIGURE 2.11: Dependence of Fermi velocity in TBG $v_F^{(TBG)}$ and in monolayer graphene $v_F^{(G)}$ with the rotation angle [45].

It is shown that the Fermi velocity in TBG is completely depleted for low angles. This effect may suggest a strong correlation between the electrons present in the flat bands, because their kinetic energy has been decreased. Indeed, strong-correlated states and superconductivity has been reported in TBG for a magic angle of 1.1° [39] (very close to the system in Figure 2.10(d)), and even though exhibit Mott-like insulator states at half filling in this magic angle [40], evidencing the strong correlation and localization of the electrons in the flat bands.

Twisted double bilayer graphene

Another interesting system of graphene multilayers is the twisted double bilayer graphene (TDBG), a tetralayer graphene structure composed of two AB stacked graphene bilayers with a relative rotation angle between them.

The band structure obtained from the TB model is shown in Figure 2.12 (a), (b) and (c) for three different rotation angles, 3.9°, 2.3° and 1.6° respectively. It is clear to note that the TDBG is a semiconductor with a gap between the valence and conduction bands, and this gap depends on the twist angle between the bilayers. Moreover, for low angles, close to the magic angle in the TBG, the system have flat bands near the Fermi Level, as is shown in Figure 2.12(c), with a rotation angle of 1.6°. This gap between the valence and conduction band becomes indirect, as marked in dashed lines in Figure 2.12(c). Figure 2.12(d) shows the angle dependence of the gap in the K point (red triangles). It shows a monotonically decreasing behavior as the rotation angle decreases, with a sharp drop for angles below 5°.

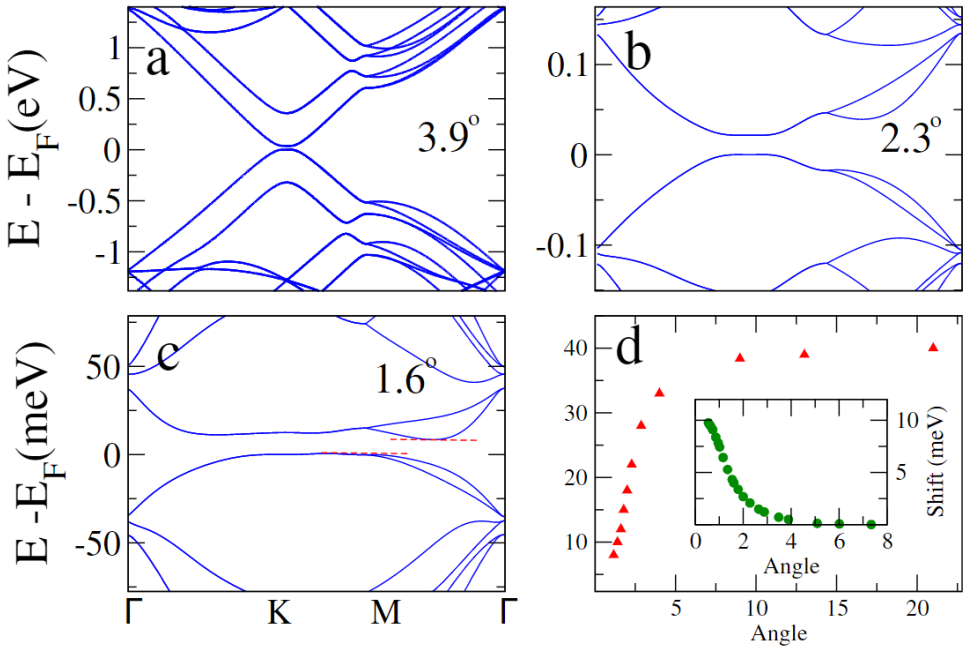


FIGURE 2.12: (a),(b),(c) Band structures of TDBG for three different rotation angles. The red dashed lines in (c) indicates the indirect gap. (d) The value of the gap as a function of the angle. In the inset shift of the Dirac cone in TBG. [46]

Moreover, the gap found in the band structure for the TDBG can be controlled by an external potential perpendicular to the layers, as shown in Fig.2.13. This is a crucial difference with the TBG [46], where an external field does not open a gap, but breaks the degeneracy of the bands by shifting one upward and the other downward one up and the other down in the applied potential value..

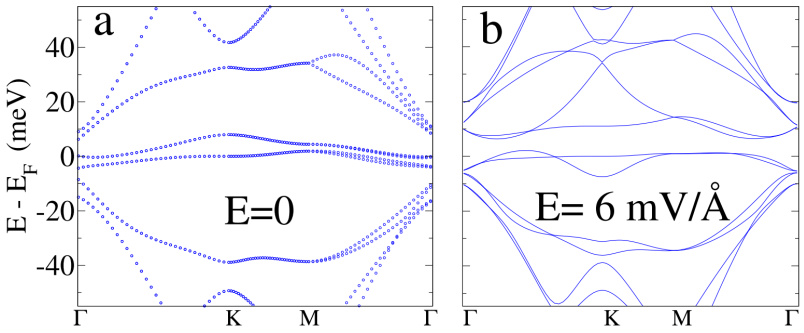


FIGURE 2.13: Band structure of TDBG for an angle of 1.16°, (a) without external electric field; (b) with a perpendicular electric field of 6 mV/Å[46].

In recent experiments at the DTBG, correlated states associated with these flat bands have been found, observing insulating states at a half-filled and quarted filled conduction band in an intermediate range of displacement fields [47–50].

2.6 Local density of states

The local density of states (LDOS) at site $\mathbf{r}$ can be obtained by the retarded Green function $G_0^{\text{ret}} = (\varepsilon - H + i\eta)^{-1}$ [51]:

$$\rho(\mathbf{r}, \varepsilon) = -\frac{1}{\pi}\text{Im}\{G_0^{\text{ret}}(\mathbf{r}, \mathbf{r}, \varepsilon)\}, \tag{2.26}$$

where η is an infinitesimal parameter. To obtain the value of the LDOS is necessary integrate in all the Brillouin zone. If this cannot be done analytically, a grid of points in the Brillouin zone can be made as suggested by Monkhorst-Pack [52]. Appendix A describes the procedure for obtaining the Monkhorst-Pack point grid.

With the definition of the LDOS, the density of states (DOS) of the system is given by

$$\mathcal{N}(\varepsilon) = -\frac{1}{\pi}\text{Im}\{\text{Tr}\{G_0^{\text{ret}}(\mathbf{r}, \mathbf{r}, \varepsilon)\}\}. \tag{2.27}$$

In two dimensions a saddle point in the electronic band structure leads to a divergence in the density of states, also known as a Van Hove singularity (VHS). When this VHS is close to the Fermi energy (E_F), interactions are magnified by the enhanced DOS, which can give rise to new phases of matter and collective phenomena [53, 54].

2.7 Electronic localization

A distinctive feature characterizing TBG is the pronounced localization of electrons in the AA region of the unit cell. This localization within the AA stacking configuration stands as a hallmark phenomenon, playing a pivotal role in the emergence of electronic correlations within the material. The majority of the charge associated with the two highest valence bands tends to concentrate in this specific region [55, 56].

To scrutinize the transformation of electronic localization with diminishing rotation angles, we employ the Tight-Binding (TB) Hamiltonian. Our focus lies in assessing the projection of states from the two highest valence bands (HVB) onto each layer, providing insights into the evolving charge distribution. This is achieved through the expression:

$$n_l = \sum_{j \in L_l} \sum_k \sum_{n \in \text{HVB}} \frac{1}{N_k} \left| \langle \Psi_{nk} | \phi_j \rangle \right|^2 \tag{2.28}$$

where Ψ_{nk} is the wavefunction of the system for an eigenvalue n at a given k point, ϕ_j is the orbital at site j, and N_k is the total number of k points used in the integration. The sum over n comprises only states in the two HVB, the sum over k represents the integration over the Brillouin zone and the sum over j includes all orbital in the layer l. The k points are selected using the Monkhorst-Pack scheme described in Appendix A and simplified by taking into account the Brillouin zone symmetry.

The resulting quantity, denoted as n_l, when multiplied by the electron charge, serves as a metric for the charge distribution associated with each layer within the aforementioned bands. Henceforth, in the following we will refer to this magnitude simply as "charge".

Analyzing the charge distribution across layers provides a nuanced perspective on how electronic states localize within the material as the rotation angle decreases.

This analysis is crucial for understanding the intricate interplay of electronic interactions in low-angle rotated graphene structures and sheds light on the emerging electronic properties of such systems.

2.8 Structural lattice relaxation

Detailed understanding of the electronic properties of two-dimensional systems requires a thorough analysis of the crystal structure, especially when the number of atoms in the unit cells is significantly large, as in the case of twisted multilayers. In real systems, the lattice structure relaxes spontaneously in order to achieve a more favorable energy structure, and this relaxation can affect the electronic properties of the system. For example, as seen in section 2.5.2, sites with AA, AB, BA or SL stacking appear in the TBG. However, the energy of an interlayer binding in an AB or BA site is lower than in an AA site [42], because the AA sites represent antibonding states, the crystal structure of the TBG will spontaneously deform in order to maximize the AB/BA areas and minimize the AA areas, and thus achieve a more favorable energetic state.

The lattice relaxation was studied computationally by density functional theory (DFT), molecular dynamics and continuum models [42, 57–60]. In this work, a structural relaxation of the network based on classical molecular dynamics simulations using the Large-scale Atomic/Molecular Massively Parallel Simulator (LAMMPS) code will be used.

2.8.1 LAMMPS molecular dynamics simulation

LAMMPS is a classical molecular dynamics (MD) code that models ensembles of particles in a liquid, solid, or gaseous state [61]. In the most general sense, LAMMPS integrates Newton's equations of motion for a collection of interacting particles. A single particle can be an atom or molecule or electron, a coarse-grained cluster of atoms, or a mesoscopic or macroscopic clump of material. The interaction models that LAMMPS includes are mostly short-ranged in nature; some long-range models are included as well.

Using LAMMPS, energy minimization was performed for non-bonded interlayer interactions using the Kolmogorov-Crespi potential [62, 63] with a cutoff of 16 Å and bonded intralayer interactions using the REBO potential [64, 65]. The relaxations were done with an energy tolerance of 10^{-10} eV per atom [66].

It is worth asking how structural relaxation affects the electronic properties of the systems. Returning to the example of the TBG, the Figure 2.14 shows the calculation of the band structure from the TB Hamiltonian for a rotation angle of 1.12° considering the unrelaxed structure in (a), and the relaxed structure in (b).

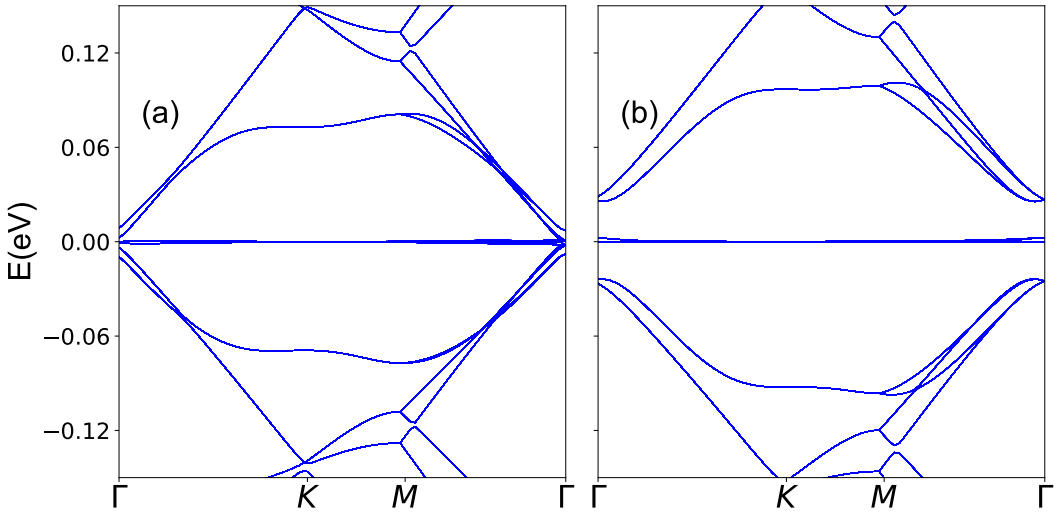


FIGURE 2.14: Band structure of the TBG for a rotation angle of 1.12° with: (a) unrelaxed structure, (b) relaxed structure.

As can be seen in the Fig. 2.14(a), the flat bands are joined to the conduction and valence bands at the Γ point. In contrast, in Fig. 2.14(b), where the structure underwent structural relaxation, the flat bands are energetically separated from the other bands. As seen in previous sections, electrons in the flat bands undergo a decrease in their Fermi velocity, which can give rise to correlated states between them. If we add to this the fact that these bands are energetically far away from each other, this results in a localization of the electrons in these bands, where an increase in energy greater than the bandwidth would be required to bring the electrons to the conduction bands. This is why it is important to take into account the structural relaxation of these systems, especially for small angles, where the number of atoms is high, and the effects can be significant. Is for this reason that in this work all the structures with rotation angles below 2° were relaxed.

2.9 Twisted double ABC trilayer graphene

In the previous sections, we have explored the wealth of emergent properties in graphene multilayer systems, from the fundamental features of monolayers to the fascinating phenomena observed in ABC trilayers and other structures with rotation. In this section, we will dive into the heart of our research: the detailed study of the electronic properties of ABC trilayers when two of them are stacked with a specific rotation angle, giving rise to the system we call "Twisted Double ABC Trilayer Graphene" (2ABCT).

The motivation for this study lies in the quest to understand how the combination of the unique properties of ABC trilayers and twist effects in double layer systems can lead to even more intriguing electronic phenomena. The ABC trilayer has proven to be a fertile field for the observation of phenomena such as superconductivity and correlated insulating states. By introducing rotation between two ABC trilayers, we hope to open the door to new possibilities and understand how complex interlayer interactions contribute to the formation of unusual electronic states.

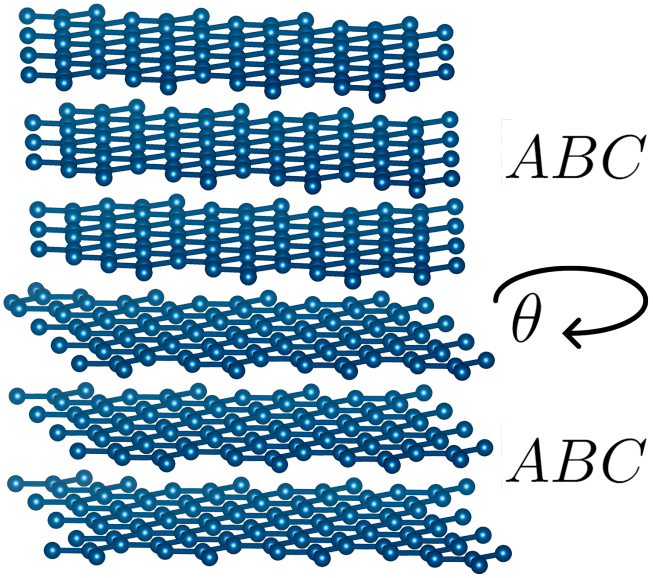


FIGURE 2.15: Configuration of twisted double ABC trilayer graphene.

The configuration of the 2ABCT is shown in Fig.2.15. Two ABC trilayers of graphene are placed on top of each other, and then rotated with respect to an angle θ, with the same procedure as is expose in section 2.5.2. The main electronic properties of this new system will be shown in the next chapter.

Chapter 3

Results

This chapter will present the main results of this thesis. First, a more detailed discussion of the electronic properties of the ABC trilayer with external field will be presented, which, as will be seen later, present a great similarity with the properties of the 2ABCT. Secondly, the electronic properties of 2ABCT will be show, specifically, its band structure and the electronic localization of this system. In order to better characterize this electronic localization in the double trilayer, the same phenomenon will be studied in a simpler system, composed of an ABA trilayer with the top layer rotated with respect to the others, which will be called ABT.

The central objective of this chapter is to scrutinize and decipher the intricate electronic structure of 2ABCT. By employing simpler models like ABT and ABC trilayers, we aim to glean insights into the behavior of the 2ABCT system, enhancing our grasp on the electronic phenomena at play. The results presented herein lay the foundation for a comprehensive understanding of the electronic intricacies within these graphene multilayer structures.

3.1 ABC trilayer graphene

It was studied in section 2.4.1 that for the graphene trilayer there are two possible stackings: ABA and ABC. Both stacking have no gap in the absence of an external field. However, there are substantial differences between them. As studied, ABA stacking with an external field causes the bands to overlap each other (see Figure 2.6), while ABC stacking with an external field causes the opening of a gap, which can be controlled from the field strength, as shown in Figure 3.1(b), which presents the band structure for an ABC trilayer with a small external field of 10meV/A in blue solid line, while the red dashed line shows the structure in the case without external field.

Another difference exists between the two stackings. As can be seen in Figure 2.5, the middle layer in the ABC has only anti-bonding type bonds with the neighboring layers. That is, this layer has more energetic bonds than the outer layers. The direct consequence of this arrangement is that states close to the Fermi level have a strong preference to be located in the outer layers and on atoms that have no close neighbors in the vertical direction. In Figure 3.1(a) it is shown a side view of the unit cell of the ABC trilayer and the localization of the states from $E_f - 0.5$ to E_F eV obtained from a DFT calculation (performed by Prof. Eric Suarez, guiding professor of this thesis) of an ABC trilayer under an external electric field to separate the valence and conduction bands. Evidently, these states predominantly inhabit the B1 and B3 atoms situated within the outer layers, strategically avoiding any immediate vertical neighbors within the middle layer (see Fig. 3.1(c)). Intriguingly, despite this spatial arrangement, the emergence of flat bands positioned a few meV from the Fermi level in both scenarios is noteworthy. The existence of such states suggests a correlation

with collective phenomena, as evidenced by various experimental observations [29, 67, 68].

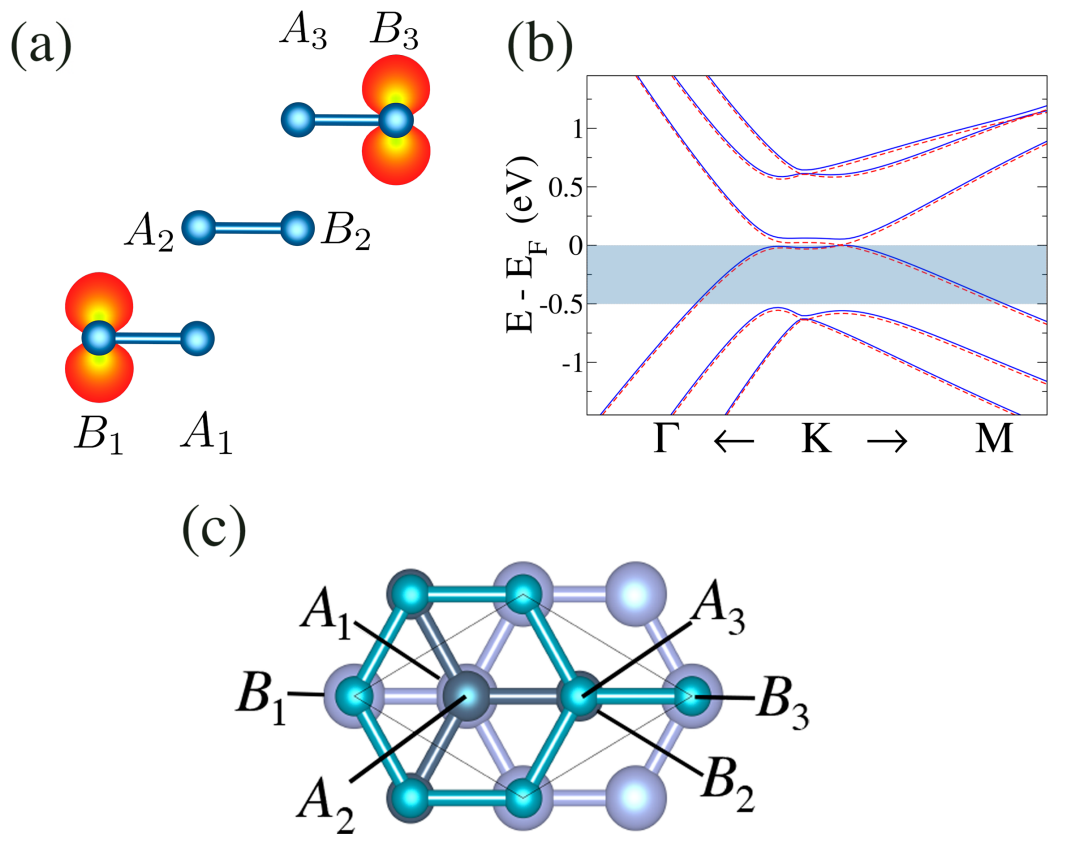


FIGURE 3.1: (a) Localization of the states in the shadow region of (b), where the electronic structure of trilayer ABC is shown around the K point. Red dashed lines are the bands without external field, and blue solid lines for $\mathbf{E} = 10\text{meV/Å}\,\hat{z}$, (c) Top view of trilayer ABC.

This finding reinforces the idea that the electronic structure of ABC trilayers is intricate and subject to complex collective phenomena. The detailed analysis of these states, in conjunction with experimental observations, will be essential to unravel the practical and theoretical implications of this remarkable electronic response. In the following sections, we will delve deeper into the analysis of these states and their connection to specific collective phenomena, thus providing a more comprehensive insight into the electronic richness of mutlilayers systems.

3.2 Electronic properties of double twisted ABC trilayer

In this section, we turn our attention to a thorough exploration of the electronic properties of the double twisted ABC trilayer (2ABCT). As we delve into the analysis of its electronic properties, we aim to unravel the unique effects of rotation on the band structure and electronic localization.

The phenomenon of *twistronics* has emerged as an exciting field, where small variations in the twisting angle between layers can have a substantial impact on the electronic properties of the system. In this context, we will explore the band structure

of 2ABCT, deciphering how rotation affects dispersion relations and contributes to the formation of flat bands or other singular phenomena.

Subsequently, we will immerse ourselves in the study of electronic localization in the context of low rotation angles. This detailed analysis will enable us to understand how low inclinations in 2ABCT can influence charge distribution and the formation of localized states. The interaction between rotation and electronic localization becomes the primary focus of this section, providing a more comprehensive insight into the inherent complexities of the double twisted ABC trilayer.

3.2.1 Band structure

In systems comprising a few number of atomic layers, the electronic structure is notably influenced by the local environment of each layer. Earlier investigations revealed that this layer-to-layer in-equivalence contributes to gap opening [46, 69]. Consequently, it is reasonable to anticipate analogous behavior in the context of two ABC trilayers with a rotational misalignment between them. This suggests that the interplay of layer-specific environments and rotational angles can engender electronic phenomena akin to those observed in single trilayers, providing a valuable insight into the intricate interlayer interactions within these multilayer graphene systems.

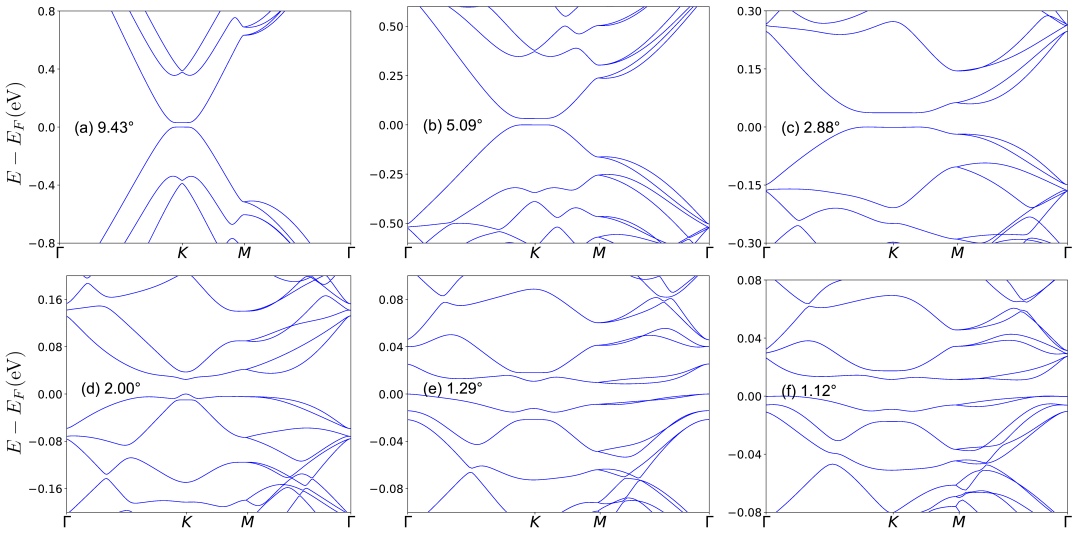


FIGURE 3.2: Band structure of 2ABCT for six rotation angles: (a) 9.43°, (b) 5.09°, (c) 2.88°, (d) 2.00°, (e) 1.20° and (f) 1.12°.

The system comprising two ABC trilayers with a rotation between them exhibits semiconductor behavior, a noteworthy characteristic despite each individual ABC trilayer being inherently non-semiconducting. Illustrated in Figure 3.2 is the band structure derived from the Tight-Binding (TB) Hamiltonian (equation (2.22)) for six distinct rotation angles (9.43°, 5.09°, 2.88°, 2.00°, 1.20°, and 1.12°). Notably, even for relatively large rotation angles, the electronic structure features discernible flat bands. This observation underscores the system's intrinsic gap, affirming its semiconducting nature.

Furthermore, the presence of flat bands persists across various rotation angles, and intriguingly, as the rotation angle diminishes, these flat bands become more pronounced. This trend suggests a nuanced interplay between interlayer rotation and

the emergence of distinctive electronic states, offering valuable insights into the delicate balance governing the electronic properties of the coupled two ABC trilayers. The persistence and enhancement of flat bands with decreasing rotation angles highlight the intricate influence of layer rotation on the electronic structure, shedding light on the subtle yet consequential electronic phenomena within this multilayer graphene system.

It is important to note that the TB Hamiltonian only allows to obtain the gap if a site energy term is added in each layer (first term of eq. (2.22)). If we add this term with a potential value obtained from the charge distribution analysis using a simple capacitor plate model, the TB result agrees with DFT calculations (permormed by Prof. Eric Suárez). In Appendix B we compare the bands structure for two angles calculated by both methods: DFT and TB.

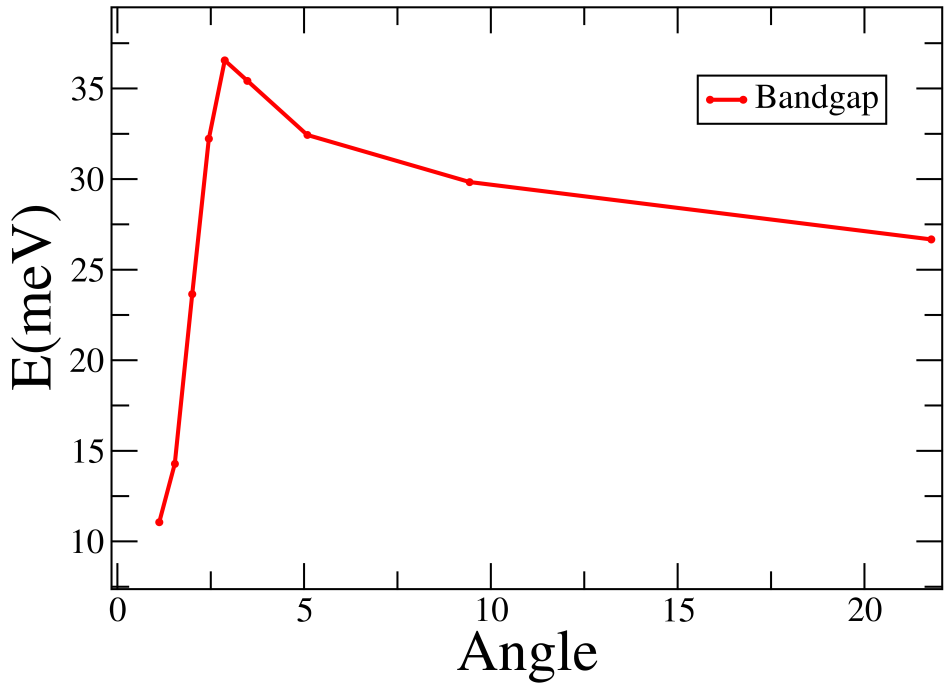


FIGURE 3.3: Value of bandgap as function of rotation angle in 2ABCT.

Figure 3.3 illustrates the variation in the bandgap concerning the rotation angle. Notably, for larger angles, the gap maintains a relatively constant value of approximately 30 meV. As the angle diminishes, there is a transient increase in the gap, peaking at 35 meV. However, for angles smaller than 2 degrees, the bandgap experiences a rapid decline, reaching an almost 10 meV minimum. The distinctive environments characterizing each layer within the system play a pivotal role in inducing this gap phenomenon. When the two ABC trilayers are coupled, the inversion symmetry, crucial for preserving the sublayer exchange symmetry of each ABC structure, is broken, leading to gap opening. This discrepancy in layer environments translates to distinct potentials within each layer, fostering the anticipation of charge transfers between layers. The breaking of inversion symmetry induces an asymmetry that manifests as the observed variation in the bandgap. Understanding these nuanced environmental influences provides essential insights into the intricate interlayer interactions governing the electronic properties of the coupled ABC trilayers.

Let's delve into the spatial localization of states within the flat band region adjacent to the Fermi level in the rotated structures. As depicted in Figure 3.4, we examine the state localization near the K point for both the two highest valence bands ((a) and (c)) and the lowest conduction bands ((b) and (d)). These state location calculations were performed using DFT by Professor Eduardo Menendez of the Universidad de Sevilla. Within the valence band, states exhibit predominant spatial localization in the intermediate layers—specifically, in the rotated layers. Even at an angle of 9.4°, there is still a lack of clear localization in the AA sites of the unit cell, although the inception of moiré pattern formation becomes perceptible. An inset in Figure 3.4(c) unveils that the states find localization in the bonding orbitals, precisely in an atom positioned at the center of the hexagon within the neighboring Bernal layer—a pattern akin to the one observed in Trilayer ABC. Notably, if the system were doped, a distinct scenario emerges: the states predominantly localize in the outer layers and, correspondingly, within the B-type atoms. This insight, illustrated in Figure 3.4(b) and (d), underscores the profound impact of doping on the spatial distribution of electronic states, offering a crucial perspective into the tunability of the electronic properties within the double twisted ABC trilayer system.

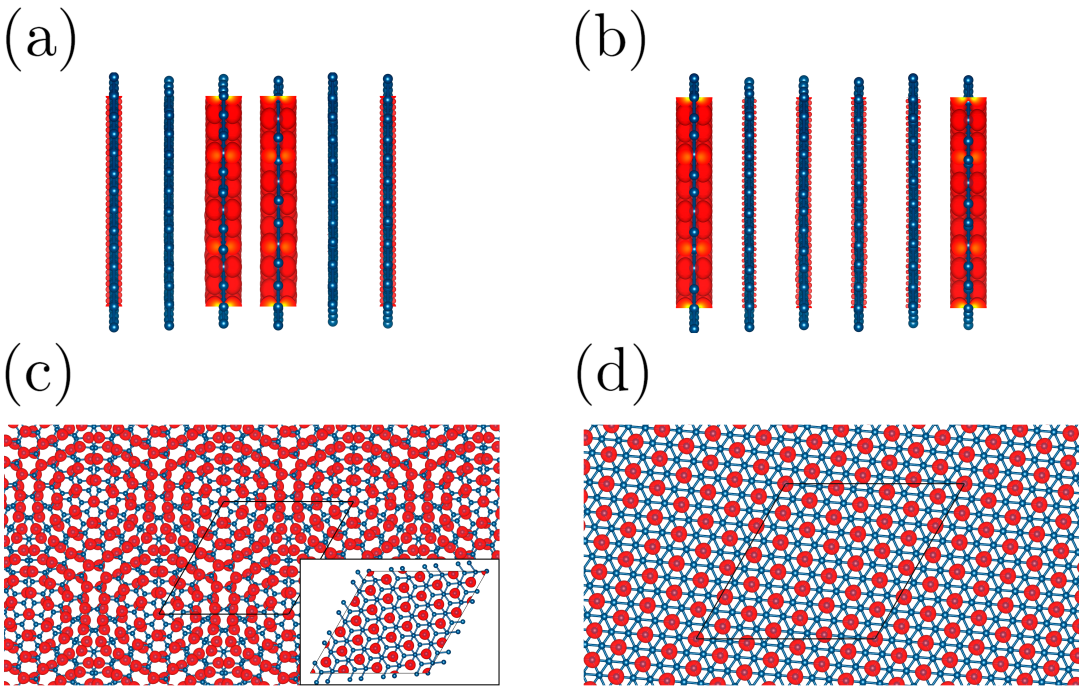


FIGURE 3.4: Side and top views of localization of states around the K point for (a), (c) for the two highest occupied valence bands, and (b), (d) for the two lowest conduction bands. Only layers 3 and 4 are shown in (c), and only layers 5 and 6 are shown in (d).

3.2.2 Electronic localization for low angles

In the exploration of electronic properties in low-angle rotated graphene structures, a key focus lies in understanding the electronic localization within the material. This section delves into the results derived from the calculation of n_l defined in eq. (2.28) for the double ABC trilayer system. As we venture into the results, the aim is to shed light on how the charge dynamically distributes across layers as the rotation angle

decreases. Particularly, the focus is on unveiling the nuances of charge localization in response to the unique stacking configurations inherent in the low-angle rotated double ABC trilayer graphene system. The ensuing discussion provides valuable insights into the emerging electronic properties of this system and contributes to a deeper understanding of the interplay of electronic interactions in such complex graphene structures.

In Figure 3.5(a), the evolution of the charge n_l associated with the two highest valence bands (HVB) unfolds as a function of the rotation angle. The inherent symmetry in the system dictates that layers 1-6, 2-5, and 3-4 exhibit identical charge values due to their symmetrical arrangements. Notably, layers 3-4, initially rotated concerning each other, witness an intriguing evolution in charge localization as the rotation angle decreases. In the early stages of angle reduction, the charge localization within layers 3-4 intensifies, reflecting the anticipated behavior observed in rotated graphene structures. However, a departure from the typical trend observed in twisted bilayer graphene becomes evident for angles below 2.5°. Contrary to the anticipated increase in charge localization within layers 3-4, a distinctive shift occurs—the charge dynamically starts escaping from these layers. Intriguingly, it is layer 1 that emerges as the predominant recipient of this redistributed charge.

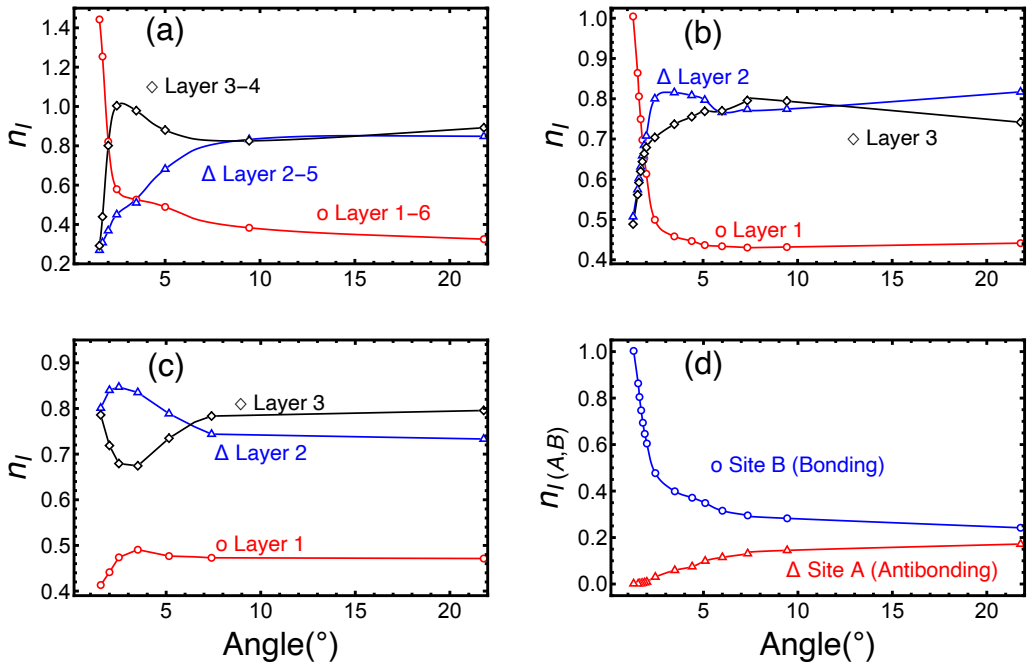


FIGURE 3.5: Charge as defined in eq. (2.28) for each layer as a function of the angle for (a) double twisted trilayer ABC, (b) Trilayer ABT, (c) Trilayer ABT with a negative external electric field. (d) n_l projected on sublattices A and B on layer 1 of trilayer ABT

In pursuit of comprehending the intriguing charge redistribution observed in the 2ABCT system, we turn our attention to a more tractable scenario—the trilayer ABA graphene system with a rotated third layer, denoted as ABT. Figure 3.5(b) illuminates that the charge dynamics in ABT parallel those observed in the more complex 2ABCT system. This parallel behavior hints at shared underlying principles governing charge redistribution in low-angle rotated trilayer graphene configurations.

To delve into the intricacies, let's dissect how the charge redistributes within

layer 1, focusing on sublattice contributions. The examination reveals a distinctive pattern: the redistributed charge predominantly congregates around the B-type bonding atoms, as illustrated in Figure 3.5(d). This observation aligns with expectations, mirroring the behavior observed in well-established configurations such as the Bernal bilayer or trilayer ABC (see Fig 3.1). The highest valence states exhibit a propensity to favor the bonding-type atoms of layer 1, offering a familiar yet insightful perspective into the charge dynamics in rotated trilayer graphene systems.

The migration of charge to the first layer, as observed in the electronic dynamics of the double ABC trilayer graphene system, can be rationalized by considering the influence of the periodic moiré potential and the interplay of electronic interactions.

The periodic moiré potential effectively confines electrons within the AA zones of the rotated layers. When an additional layer is introduced, it introduces an extra coupling option for the electron. To grasp this concept intuitively, one can envision the electron's energy increasing in the AA region due to Coulomb repulsion. Faced with this energetic challenge, the electron exhibits a preference for transitioning to another lower-energy state. In the context of the system under consideration, this lower-energy state manifests in layer one, specifically favoring the B-type atoms. This rationalization aligns with the notion that electrons, subject to Coulombic forces and the intricate potential landscape of rotated layers, seek energetically favorable configurations. The introduction of an extra layer provides an alternative pathway for charge migration, and the charge gravitates toward the first layer, specifically favoring the B-type atoms within that layer.

Furthermore, the introduction of a negative external electric field serves as a noteworthy factor in preserving charge localization in the upper layers of the trilayer ABT system. Figure 3.5(c) illustrates the charge localization in trilayer ABT under an external negative electric field $\mathbf{E} = 20\text{meV}$ along the z-axis. However, it's crucial to highlight that this localized charge, while influenced by the external field, does not reach the level observed in twisted bilayer graphene [55]. This discrepancy in charge localization underscores the distinctive electronic nature of the rotated trilayer ABT system, further emphasizing the intricate interplay of factors influencing its electronic properties.

The precise occurrence of the abrupt change in charge distribution at a specific rotation angle warrants a detailed analysis that, regrettably, exceeds the scope of this thesis. Nevertheless, to offer a conceptual framework for understanding these results, we employ a simplified toy model.

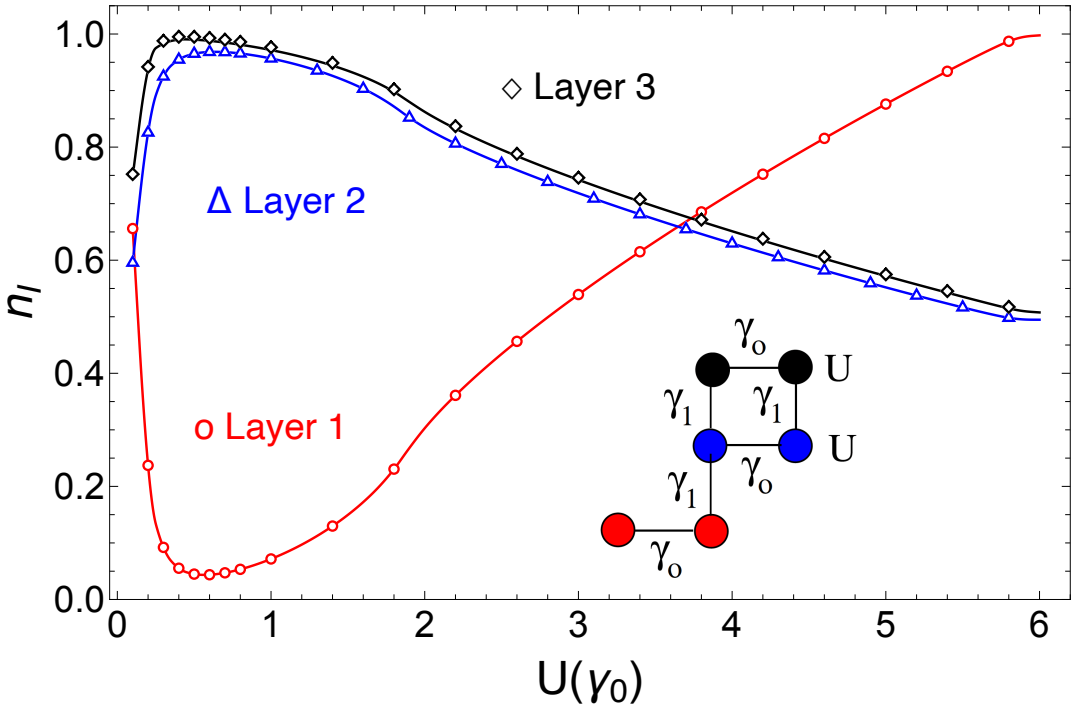


FIGURE 3.6: Charge redistribution as a function of U in each layer of a toy model: Three graphene layers with stacking ABB, with an onsite energy U on layers 2-3. In the scheme, γ_0 and γ_1 are intra and interlayer hoppings of graphene.

Toy model

Consider a structure with ABB stacking, featuring typical intra- and interlayer hopping in graphene. Introduce a U-site potential in layers 2-3, corresponding to BB stacking, thereby simulating an increase in electron energy within those layers. This increase in U is akin to a reduction in the rotation angle. Figure 3.6 schematically represents this model, and the charge associated with the last two valence bands is calculated and plotted as a function of U. As depicted in Fig. 3.6, the initial state reveals higher charge accumulation in the BB layers (layers 2 and 3). However, for U values exceeding $\sim \gamma_0/2$ eV, a discernible reversal occurs. The charge progressively accumulates more in the first layer for larger U values, precisely mirroring the observed behavior in the rotated trilayer ABT system.

While this toy model simplifies the complex dynamics at play, it provides a conceptual foundation for understanding how changes in electron energy and interlayer potentials influence charge redistribution. The reversal observed in the toy model aligns with the abrupt change witnessed in the rotated trilayer ABT system, offering a qualitative explanation for the observed phenomenon. Further investigations and detailed analyses are essential to fully grasp the intricacies of this transition and its implications for the electronic properties of low-angle rotated trilayer graphene structures.

Chapter 4

Conclusion and outlook

In this thesis, our investigation into the electron localization within a system comprising two ABC trilayers, each rotated concerning the other, has revealed intriguing semiconductor behavior and flat bands for large rotation angles. The spontaneous gap opening, attributed to the crystal field, mirrors the characteristics observed in an ABC trilayer under the influence of a slight external field. However, as the rotation angle diminishes to less than two degrees, a departure from the conventional pattern is observed. Unlike twisted bilayer graphene, where electrons predominantly concentrate in the AA region, in our system, electrons exhibit an unexpected trend, escaping towards the outer layers.

This distinctive behavior is attributed to the presence of an additional coupling, providing an avenue for electrons to transition to lower energy states. We posit that this phenomenon arises due to increased Coulomb interaction, causing the energy of electrons to rise. The system's resemblance to an ABT system (comprising three layers with ABA stacking and the last layer rotated) further elucidates this behavior. Interestingly, the application of a negative electric field successfully prevents charge leakage from the rotated layers.

Our study underscores that the charge escape from the rotated layers correlates with an elevation in electron energy in those layers, influenced by Coulomb interaction. The insights gained from a toy model underscore the reproducibility of this charge behavior by manipulating the energy levels of specific layers. These findings not only raise compelling questions for further exploration in both 2ABCT and ABT systems but also offer a captivating avenue to comprehend the origins of superconductivity in graphene-based layer systems. The intricate interplay of factors and the distinctive electronic behaviors unveiled in this research open avenues for continued exploration and refinement in understanding the fascinating properties of these layered graphene structures.

Appendix A

Monkhorst-Pack special points grid

The Monkhorst-Pack (MP) method [52] provides an efficient approach for generating a set of special points in the Brillouin zone, crucial for electronic structure calculations in solid-state physics. These special points are instrumental in numerically approximating integrals over the Brillouin zone, enabling accurate calculations of various physical properties. The grid of special points is determined by the equation

$$\mathbf{k}_{n_1,n_2,n_3} = \sum_{i}^{3} \frac{2n_i - N_i - 1}{2N_i} \mathbf{b}_i, \tag{A.1}$$

where $\mathbf{k}$ represents a special point, $\mathbf{b}_i$ are the reciprocal lattice vectors, N_i are the number of points along each reciprocal lattice vector and $n_i = 1, 2, \ldots, N_i$.

The MP method stands as a pivotal strategy in the realm of electronic structure calculations within solid-state physics. By furnishing a well-defined grid of special points in the Brillouin zone, it facilitates the numerical approximation of integrals critical for determining various physical properties. The uniform sampling inherent in the MP method ensures a judicious representation of the Brillouin zone, eliminating unnecessary computational redundancy. This leads to a notable enhancement in computational efficiency, a particularly advantageous feature when dealing with extensive and intricate unit cells.

Beyond computational expediency, the MP method plays a crucial role in preserving integration accuracy. Through the strategic selection of k-points, it enables precise calculations of density of states and band structures. Importantly, the method strikes a balance between computational resources and result accuracy, making it an invaluable tool in electronic structure studies. Exploiting the crystalline symmetry of materials further refines this approach. The concept of irreducible representation allows for a reduction in the number of k-points while retaining accuracy, offering researchers a powerful means to explore electronic and structural properties in a computationally efficient manner.

A.1 Crystal symmetry

The crystalline symmetry of the material offers an opportunity to further reduce the number of k-points without compromising accuracy. The concept of irreducible representation comes into play. If a k-point $\mathbf{k}$ belongs to a certain symmetry class, its equivalent counterparts under symmetry operations R_n will yield the same physical quantity. Thus, the grid can be reduced by considering only irreducible points.

For example, in graphene, where the hexagonal lattice possesses sixfold rotational symmetry, the number of k-points can be reduced by a factor of six. This reduction is achieved by considering only one-sixth of the Brillouin zone and replicating the calculated quantities accordingly

Appendix B

Comparison of TB and DFT calculations

In Figure B.1, a compelling comparison of the electronic structures at low energies between the DFT and TB calculations is presented for rotation angles of 13.1 and 21.7 degrees. The remarkable agreement observed between these two methodologies reinforces the reliability of our theoretical framework. It's noteworthy that the system exhibits semiconductor behavior, with distinct flat bands near the Fermi level, underscoring the precision of our computational models in capturing the essential electronic features. This semiconductor nature holds significant implications for potential applications and further emphasizes the consistency between the DFT and TB results.

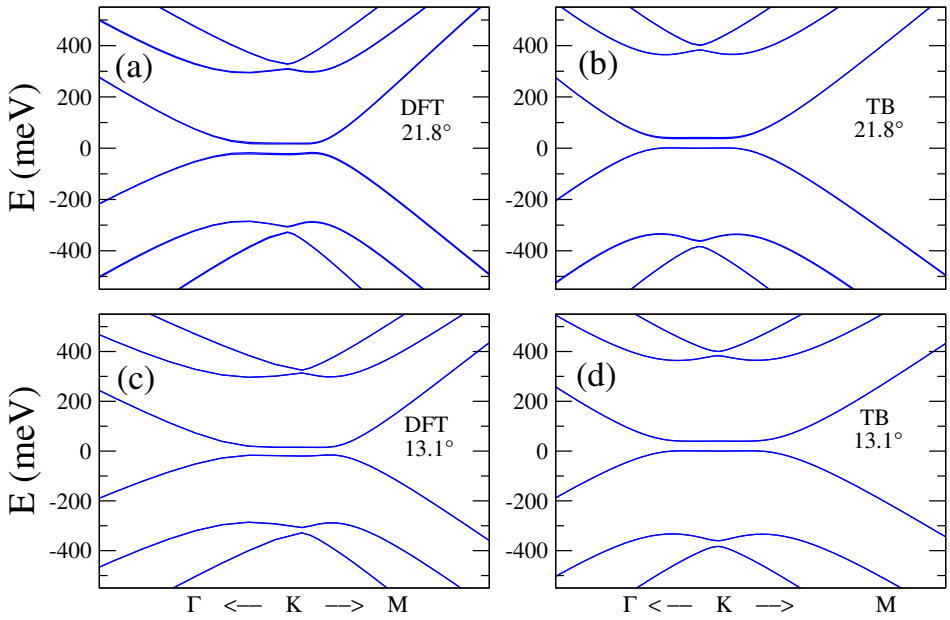


FIGURE B.1: Comparison of DFT (left panels) and TB (right panels) calculated bands around the K point. The top rows for a relative rotation angle $\theta = 21.8°$ and the bottom rows for $\theta = 13.1°$.

Bibliography

[1] K. S. Novoselov et al. "Electric Field Effect in Atomically Thin Carbon Films". In: *Science* 306.5696 (2004), pp. 666–669. DOI: 10.1126/science.1102896.

[2] Daniel R. Cooper et al. "Experimental review of graphene". In: (Oct. 2011).

[3] S. Das Sarma, Shaffique Adam, E. H. Hwang, and Enrico Rossi. "Electronic transport in two-dimensional graphene". In: *Reviews of Modern Physics* 83 (2 May 2011), pp. 407–470. ISSN: 00346861. DOI: 10.1103/RevModPhys.83.407.

[4] K. S. Novoselov et al. "Two-dimensional gas of massless Dirac fermions in graphene". In: *Nature* 438.7065 (2005), pp. 197–200. ISSN: 1476-4687. DOI: 10.1038/nature04233.

[5] A. H. Castro Neto, F. Guinea, N. M.R. Peres, K. S. Novoselov, and A. K. Geim. "The electronic properties of graphene". In: *Reviews of Modern Physics* 81 (1 Jan. 2009), pp. 109–162. ISSN: 00346861. DOI: 10.1103/RevModPhys.81.109.

[6] Mark Wilson. *Electrons in atomically thin carbon sheets behave like massless particles*. Jan. 2006. DOI: 10.1063/1.2180163.

[7] Umesha Mogera and Giridhar U. Kulkarni. *A new twist in graphene research: Twisted graphene*. Jan. 2020. DOI: 10.1016/j.carbon.2019.09.053.

[8] Edward McCann and Mikito Koshino. "The electronic properties of bilayer graphene". In: (May 2012). DOI: 10.1088/0034-4885/76/5/056503.

[9] Mikito Koshino and Edward McCann. "Parity and valley degeneracy in multilayer graphene". In: *Physical Review B - Condensed Matter and Materials Physics* 81 (11 Mar. 2010). ISSN: 10980121. DOI: 10.1103/PhysRevB.81.115315.

[10] Sylvain Latil and Luc Henrard. "Charge carriers in few-layer graphene films". In: *Physical Review Letters* 97 (3 2006). ISSN: 00319007. DOI: 10.1103/PhysRevLett.97.036803.

[11] Ahmed Missaoui, Jouda Jemaa Khabthani, Nejm-Eddine Jaidane, Didier Mayou, and Guy Trambly de Laissardière. "Numerical analysis of electronic conductivity in graphene with resonant adsorbates: comparison of monolayer and Bernal bilayer". In: *The European Physical Journal B* 90.4 (2017), p. 75. ISSN: 1434-6036. DOI: 10.1140/epjb/e2017-70664-0.

[12] Yuanbo Zhang et al. "Direct observation of a widely tunable bandgap in bilayer graphene". In: *Nature* 459 (7248 June 2009), pp. 820–823. ISSN: 00280836. DOI: 10.1038/nature08105.

[13] Eduardo V. Castro et al. "Biased bilayer graphene: Semiconductor with a gap tunable by the electric field effect". In: *Physical Review Letters* 99 (21 Nov. 2007). ISSN: 00319007. DOI: 10.1103/PhysRevLett.99.216802.

[14] Kin Fai Mak, Chun Hung Lui, Jie Shan, and Tony F. Heinz. "Observation of an electric-field-induced band gap in bilayer graphene by infrared spectroscopy". In: *Physical Review Letters* 102 (25 June 2009). ISSN: 00319007. DOI: 10.1103/PhysRevLett.102.256405.

[15] Wenjing Zhang et al. "Opening an electrical band gap of bilayer graphene with molecular doping". In: *ACS Nano* 5 (9 Sept. 2011), pp. 7517–7524. ISSN: 19360851. DOI: 10.1021/nn202463g.

[16] Jaesung Park et al. "Single-gate bandgap opening of bilayer graphene by dual molecular doping". In: *Advanced Materials* 24 (3 Jan. 2012), pp. 407–411. ISSN: 09359648. DOI: 10.1002/adma.201103411.

[17] Haoxin Zhou et al. "Isospin magnetism and spin-polarized superconductivity in Bernal bilayer graphene". In: *Science* 375.6582 (2022), pp. 774–778. DOI: 10.1126/science.abm8386. eprint: https://www.science.org/doi/pdf/10.1126/science.abm8386. URL: https://www.science.org/doi/abs/10.1126/science.abm8386.

[18] Yiran Zhang et al. "Enhanced superconductivity in spin–orbit proximitized bilayer graphene". In: *Nature* 613.7943 (2023), pp. 268–273. ISSN: 1476-4687. DOI: 10.1038/s41586-022-05446-x. URL: https://doi.org/10.1038/s41586-022-05446-x.

[19] Chun Hung Lui, Zhiqiang Li, Kin Fai Mak, Emmanuele Cappelluti, and Tony F. Heinz. "Observation of an electrically tunable band gap in trilayer graphene". In: *Nature Physics* 7 (12 2011), pp. 944–947. ISSN: 17452481. DOI: 10.1038/NPHYS2102.

[20] Yi Ping Lin, Jei Wang, Jian Ming Lu, Chiun Yan Lin, and Ming Fa Lin. "Energy spectra of ABC-stacked trilayer graphene in magnetic and electric fields". In: *RSC Advances* 4 (100 2014), pp. 56552–56560. ISSN: 20462069. DOI: 10.1039/c4ra10860d.

[21] Mikito Koshino. "Interlayer screening effect in graphene multilayers with ABA and ABC stacking". In: *Physical Review B - Condensed Matter and Materials Physics* 81 (12 Mar. 2010). ISSN: 10980121. DOI: 10.1103/PhysRevB.81.125304.

[22] Fan Zhang, Bhagawan Sahu, Hongki Min, and Allan H. MacDonald. "Band Structure of ABC-Stacked Graphene Trilayers". In: (Apr. 2010). DOI: 10.1103/PhysRevB.82.035409.

[23] M. F. Craciun et al. "Trilayer graphene is a semimetal with a gate-tunable band overlap". In: *Nature Nanotechnology* 4 (6 2009), pp. 383–388. ISSN: 17483395. DOI: 10.1038/nnano.2009.89.

[24] S. H. Jhang et al. "Stacking-order dependent transport properties of trilayer graphene". In: *Physical Review B - Condensed Matter and Materials Physics* 84 (16 Oct. 2011). ISSN: 10980121. DOI: 10.1103/PhysRevB.84.161408.

[25] W. Bao et al. "Stacking-dependent band gap and quantum transport in trilayer graphene". In: *Nature Physics* 7 (12 2011), pp. 948–952. ISSN: 17452481. DOI: 10.1038/NPHYS2103.

[26] K. Zou, Fan Zhang, C. Clapp, A. H. MacDonald, and J. Zhu. "Transport studies of dual-gated ABC and ABA trilayer graphene: Band gap opening and band structure tuning in very large perpendicular electric fields". In: *Nano Letters* 13 (2 Feb. 2013), pp. 369–373. ISSN: 15306984. DOI: 10.1021/nl303375a.

[27] Tymofiy Khodkov, Ivan Khrapach, Monica Felicia Craciun, and Saverio Russo. "Direct Observation of a Gate Tunable Band Gap in Electrical Transport in ABC-Trilayer Graphene". In: *Nano Letters* 15 (7 July 2015), pp. 4429–4433. ISSN: 15306992. DOI: 10.1021/acs.nanolett.5b00772.

[28] Matthew Yankowitz, Fenglin Wang, Chun Ning Lau, and Brian J. LeRoy. "Local Spectroscopy of the Electrically Tunable Band Gap in Trilayer Graphene". In: (Jan. 2013). DOI: 10.1103/PhysRevB.87.165102.

[29] Haoxin Zhou, Tian Xie, Takashi Taniguchi, Kenji Watanabe, and Andrea F. Young. "Superconductivity in rhombohedral trilayer graphene". In: *Nature* 598 (7881 Oct. 2021), pp. 434–438. ISSN: 14764687. DOI: 10.1038/s41586-021-03926-0.

[30] Yang-Zhi Chou, Fengcheng Wu, Jay D. Sau, and Sankar Das Sarma. "Acoustic-phonon-mediated superconductivity in rhombohedral trilayer graphene". In: (June 2021). DOI: 10.1103/PhysRevLett.127.187001.

[31] Huijia Dai, Junchen Hou, Xiao Zhang, Ying Liang, and Tianxing Ma. "Mott insulating state and d+id superconductivity in an ABC graphene trilayer". In: *Physical Review B* 104 (3 July 2021). ISSN: 24699969. DOI: 10.1103/PhysRevB.104.035104.

[32] Zhiyu Dong and Leonid Levitov. "Superconductivity in the vicinity of an isospin-polarized state in a cubic Dirac band". In: (Sept. 2021).

[33] Areg Ghazaryan, Tobias Holder, Maksym Serbyn, and Erez Berg. "Unconventional Superconductivity in Systems with Annular Fermi Surfaces: Application to Rhombohedral Trilayer Graphene". In: *Physical Review Letters* 127 (24 Dec. 2021). ISSN: 10797114. DOI: 10.1103/PhysRevLett.127.247001.

[34] Shubhayu Chatterjee, Taige Wang, Erez Berg, and Michael P. Zaletel. "Intervalley coherent order and isospin fluctuation mediated superconductivity in rhombohedral trilayer graphene". In: (Aug. 2021). DOI: 10.1038/s41467-022-33561-w.

[35] Tommaso Cea, Pierre A. Pantaleón, Vo Tien Phong, and Francisco Guinea. "Superconductivity from Repulsive Interactions in Rhombohedral Trilayer Graphene: a Kohn-Luttinger-Like Mechanism". In: (Sept. 2021). DOI: 10.1103/PhysRevB.105.075432.

[36] Leo J. McGilly et al. "Visualization of moiré superlattices". In: *Nature Nanotechnology* 15 (7 July 2020), pp. 580–584. ISSN: 17483395. DOI: 10.1038/s41565-020-0708-3.

[37] Feng He et al. *Moiré Patterns in 2D Materials: A Review*. Apr. 2021. DOI: 10.1021/acsnano.0c10435.

[38] Eva Y. Andrei et al. *The marvels of moiré materials*. Mar. 2021. DOI: 10.1038/s41578-021-00284-1.

[39] Yuan Cao et al. "Unconventional superconductivity in magic-angle graphene superlattices". In: *Nature* 556 (7699 Apr. 2018), pp. 43–50. ISSN: 14764687. DOI: 10.1038/nature26160.

[40] Yuan Cao et al. "Correlated insulator behaviour at half-filling in magic-angle graphene superlattices". In: *Nature* 556 (7699 Apr. 2018), pp. 80–84. ISSN: 14764687. DOI: 10.1038/nature26154.

[41] J. M. Campanera, G. Savini, I. Suarez-Martinez, and M. I. Heggie. "Density functional calculations on the intricacies of Moiré patterns on graphite". In: *Physical Review B - Condensed Matter and Materials Physics* 75 (23 June 2007). ISSN: 10980121. DOI: 10.1103/PhysRevB.75.235449.

[42] Nguyen N.T. Nam and Mikito Koshino. "Lattice relaxation and energy band modulation in twisted bilayer graphene". In: *Physical Review B* 96 (7 Aug. 2017). ISSN: 24699969. DOI: 10.1103/PhysRevB.96.075311.

[43] Leon Balents, Cory R. Dean, Dmitri K. Efetov, and Andrea F. Young. "Superconductivity and strong correlations in moiré flat bands". In: *Nature Physics* 16.7 (2020), pp. 725–733. ISSN: 1745-2481. DOI: 10.1038/s41567-020-0906-9. URL: https://doi.org/10.1038/s41567-020-0906-9.

[44] Youngjoon Choi et al. "Electronic correlations in twisted bilayer graphene near the magic angle". In: *Nature Physics* 15.11 (2019), pp. 1174–1180. ISSN: 1745-2481. DOI: 10.1038/s41567-019-0606-5. URL: https://doi.org/10.1038/s41567-019-0606-5.

[45] E. Suárez Morell, J. D. Correa, P. Vargas, M. Pacheco, and Z. Barticevic. "Flat bands in slightly twisted bilayer graphene: Tight-binding calculations". In: *Physical Review B - Condensed Matter and Materials Physics* 82 (12 Sept. 2010). ISSN: 10980121. DOI: 10.1103/PhysRevB.82.121407.

[46] F. J. Culchac, R. R. Del Grande, Rodrigo B. Capaz, Leonor Chico, and E. Suárez Morell. "Flat bands and gaps in twisted double bilayer graphene". In: *Nanoscale* 12 (8 2020), pp. 5014–5020. DOI: 10.1039/C9NR10830K.

[47] Cheng Shen et al. "Correlated states in twisted double bilayer graphene". In: *Nature Physics* 16 (5 May 2020), pp. 520–525. ISSN: 17452481. DOI: 10.1038/s41567-020-0825-9.

[48] Xiaomeng Liu et al. "Tunable spin-polarized correlated states in twisted double bilayer graphene". In: *Nature* 583 (7815 July 2020), pp. 221–225. ISSN: 14764687. DOI: 10.1038/s41586-020-2458-7.

[49] G. William Burg et al. "Correlated Insulating States in Twisted Double Bilayer Graphene". In: *Physical Review Letters* 123 (19 Nov. 2019). ISSN: 10797114. DOI: 10.1103/PhysRevLett.123.197702.

[50] Yuan Cao et al. "Tunable correlated states and spin-polarized phases in twisted bilayer–bilayer graphene". In: *Nature* 583 (7815 July 2020), pp. 215–220. ISSN: 14764687. DOI: 10.1038/s41586-020-2260-6.

[51] Eleftherios N. Economou. *Green's functions in Quantum Physics*. Third Edition. Springer-Verlag Berlin Heidelberg New York, 2006.

[52] Hendrik J Monkhorst and James D Pack. *Special points for Brillonin-zone integrations**. 1976.

[53] Guohong Li et al. "Observation of Van Hove singularities in twisted graphene layers". In: *Nature Physics* 6 (2 2010), pp. 109–113. ISSN: 17452481. DOI: 10.1038/nphys1463.

[54] Philipp Rosenzweig, Hrag Karakachian, Dmitry Marchenko, Kathrin Küster, and Ulrich Starke. "Overdoping Graphene beyond the van Hove Singularity". In: *Physical Review Letters* 125 (17 Oct. 2020). ISSN: 10797114. DOI: 10.1103/PhysRevLett.125.176403.

[55] G. Trambly De Laissardière, D. Mayou, and L. Magaud. "Numerical studies of confined states in rotated bilayers of graphene". In: *Physical Review B - Condensed Matter and Materials Physics* 86 (12 Sept. 2012). ISSN: 10980121. DOI: 10.1103/PhysRevB.86.125413.

[56] Mikito Koshino et al. "Maximally Localized Wannier Orbitals and the Extended Hubbard Model for Twisted Bilayer Graphene". In: *Physical Review X* 8 (3 Sept. 2018). ISSN: 21603308. DOI: 10.1103/PhysRevX.8.031087.

[57] M. Angeli et al. "Emergent D6 symmetry in fully relaxed magic-angle twisted bilayer graphene". In: *Physical Review B* 98 (23 Dec. 2018). ISSN: 24699969. DOI: 10.1103/PhysRevB.98.235137.

[58] Francisco Guinea and Niels R. Walet. "Continuum models for twisted bilayer graphene: Effect of lattice deformation and hopping parameters". In: *Physical Review B* 99 (20 May 2019). ISSN: 24699969. DOI: 10.1103/PhysRevB.99.205134.

[59] Stephen Carr et al. "Relaxation and domain formation in incommensurate two-dimensional heterostructures". In: *Physical Review B* 98 (22 Dec. 2018). ISSN: 24699969. DOI: 10.1103/PhysRevB.98.224102.

[60] Giovanni Cantele et al. "Structural relaxation and low-energy properties of twisted bilayer graphene". In: *Physical Review Research* 2 (4 Oct. 2020). ISSN: 26431564. DOI: 10.1103/PhysRevResearch.2.043127.

[61] A. P. Thompson et al. "LAMMPS - a flexible simulation tool for particle-based materials modeling at the atomic, meso, and continuum scales". In: *Comp. Phys. Comm.* 271 (2022), p. 108171. DOI: 10.1016/j.cpc.2021.108171.

[62] A. N. Kolmogorov and V. H. Crespi. "Registry-dependent interlayer potential for graphitic systems". In: *Phys. Rev. B* 71 (2005), p. 235415. DOI: 10.1103/PhysRevB.71.235415.

[63] W. Ouyang, D. Mandelli, M. Urbakh, and O. Hod. "Nanoserpents: Graphene Nanoribbon Motion on Two-Dimensional Hexagonal Materials". In: *Nano Lett.* 18 (2018), pp. 6009–6016. DOI: 10.1021/acs.nanolett.8b02848.

[64] D.W. Brenner et al. "A second-generation reactive empirical bond order (REBO) potential energy expression for hydrocarbons". In: *J. Phys. - Condens. Mat.* 14 (2003), p. 783. DOI: 10.1088/0953-8984/14/4/312.

[65] S.J. Stuart, A. B. Tutein, and J. A. Harrison. "A reactive potential for hydrocarbons with intermolecular interactions". In: *J. Chem. Phys.* 112 (2000), p. 6472. DOI: 10.1063/1.481208.

[66] Xia Liang et al. "Effect of bilayer stacking on the atomic and electronic structure of twisted double bilayer graphene". In: *Phys. Rev. B* 102 (15 2020), p. 155146. DOI: 10.1103/PhysRevB.102.155146.

[67] Haoxin Zhou et al. "Half- and quarter-metals in rhombohedral trilayer graphene". In: *Nature* 598.7881 (2021), pp. 429–433. DOI: 10.1038/s41586-021-03938-w.

[68] Yongjin Lee et al. "Gate-Tunable Magnetism and Giant Magnetoresistance in Suspended Rhombohedral-Stacked Few-Layer Graphene". In: *Nano Letters* 22.13 (2022), pp. 5094–5099. ISSN: 1530-6984. DOI: 10.1021/acs.nanolett.2c00466.

[69] E. Suárez Morell, M. Pacheco, L. Chico, and L. Brey. "Electronic Properties of Twisted Trilayer Graphene". In: (Jan. 2013). DOI: 10.1103/PhysRevB.87.125414.